Protracted late Neoproterozic – early Palaeozoic deformation and cooling history of Sør Rondane, East Antarctica, from ^{40}Ar/^{39}Ar and U–Pb geochronology

Original Article

Antonia S Ruppel[1] , Joachim Jacobs[2], Andreas Läufer[1], Lothar Ratschbacher[3], Jörg A Pfänder[3], Benita-Lisette Sonntag[3], Katarzyna Krasniqi[1], Marlina Elburg[4], Nicole Krohne[5], Detlef Damaske[1] and Frank Lisker[5]

[1]Federal Institute for Geosciences and Natural Resources (BGR), Stilleweg 2, 30655 Hannover, Germany; [2]University of Bergen, Department of Earth Science, PO Box 7800, 5020 Bergen, Norway; [3]TU Bergakademie Freiberg, 09599 Freiberg, Germany; [4]University of Johannesburg, PO Box 524 Auckland Park 2006 Johannesburg, South Africa and [5]University of Bremen, Klagenfurter Str. 2, 28359 Bremen, Germany

Abstract

^{40}Ar/^{39}Ar and U–Pb data from five structural domains constrain the late Neoproterozoic – early Palaeozoic tectonothermal history of the eastern part of the East African–Antarctic Orogen in Sør Rondane. A total of 27 new Ar/Ar ages span 570–474 Ma, roughly corresponding to the age range of three generations of syn- to post-tectonic granitoids. The ages are distinct for the five structural domains. The oldest cooling ages come from the weakly deformed southern part of the SW Terrane of Sør Rondane (SW Terrane S), a sliver of a Tonian island arc, which escaped much of the late Neoproterozoic accretionary deformation. This terrane was intruded by the oldest and largest granitoid complex at *c.* 640–620 Ma. The oldest Ar/Ar amphibole and biotite ages of 570–524 Ma are from the Main Shear Zone, along the northern margin of the SW Terrane S sliver. It hosts granites of age *c.* 584–570 Ma strung out along the shear zone. Two younger granitoid phases are recorded in the adjacent four terranes to the west, north and east of the SW Terrane S, and correlate with the younger group of Ar/Ar biotite ages spanning 513–474 Ma. We interpret the magmatic and cooling history of duration > 150 Ma to reflect repeated phases of accretion, magmatism and reactivation, that is, collage-style tectonism, partly pre-dating the incorporation of Sør Rondane into Gondwana. The study area first accreted to the cryptic Valkyrie Craton in Tonian times, was then 'sandwiched' between the Kalahari and Indo-Antarctica cratons, and experienced extensional tectonics and elevated heat flux due to lithospheric delamination, which resulted in slow cooling during the Pan-African Orogeny.

CAMBRIDGE
UNIVERSITY PRESS

1. Introduction

Sør Rondane in Dronning Maud Land (DML) is located in a key region of East Antarctica and is crucial for understanding the final amalgamation of Gondwana. Two models aim to explain the final collision. Jacobs & Thomas (2004) proposed a Himalayan-style continental collision that resulted in the formation of the late Neoproterozoic – early Palaeozoic East African–Antarctic Orogen (EAAO) (Fig. 1a, c). In the EAAO, remnants of the Mozambique Ocean, that is, the Tonian Oceanic Arc Super Terrane (TOAST; Jacobs *et al.* 2015), are sandwiched between the Kalahari craton (Namaqua–Natal Belt, Proto-Kalahari, Maud Belt, Nampula Complex) and Indo-Antarctica (Indian cratons, Napier Craton, Lützow–Holm Belt, Rayner Belt, Madagascar, Sri Lanka, Ruker Craton). The eastern margin of the Kalahari craton and the western boundary of the TOAST are delineated by the Forster Magnetic Anomaly (Riedel *et al.* 2013; Jacobs *et al.* 2015, 2020), whereas the eastern boundary of the TOAST is transitional in character and is located east of the Yamato Mountains with its continuation found in Sri Lanka and Madagaskar (Boger *et al.* 2015; Ruppel *et al.*, 2018). An alternative model interprets the Sør Rondane region as part of the E–W-trending Kuunga Orogen (e.g. Meert, 2003), in which large parts of DML, including Sør Rondane, constitute a mega-nappe rooting in northern Mozambique (e.g. Meert, 2003; Grantham *et al.* 2013) (Fig. 1b).

Sør Rondane comprises extensive rock exposures at 1000–3300 m elevation that follow a continental margin-parallel escarpment *c.* 200 km inland of the coastline (Fig. 2). Previous geological studies by Belgian (e.g. Picciotto *et al.* 1964; Van Autenboer *et al.* 1964; Van Autenboer, 1969) and Japanese (e.g. Shiraishi *et al.* 2008; Grantham *et al.* 2013; Higashino *et al.* 2013; Osanai *et al.* 2013) expeditions focused on orogenic processes related to the final
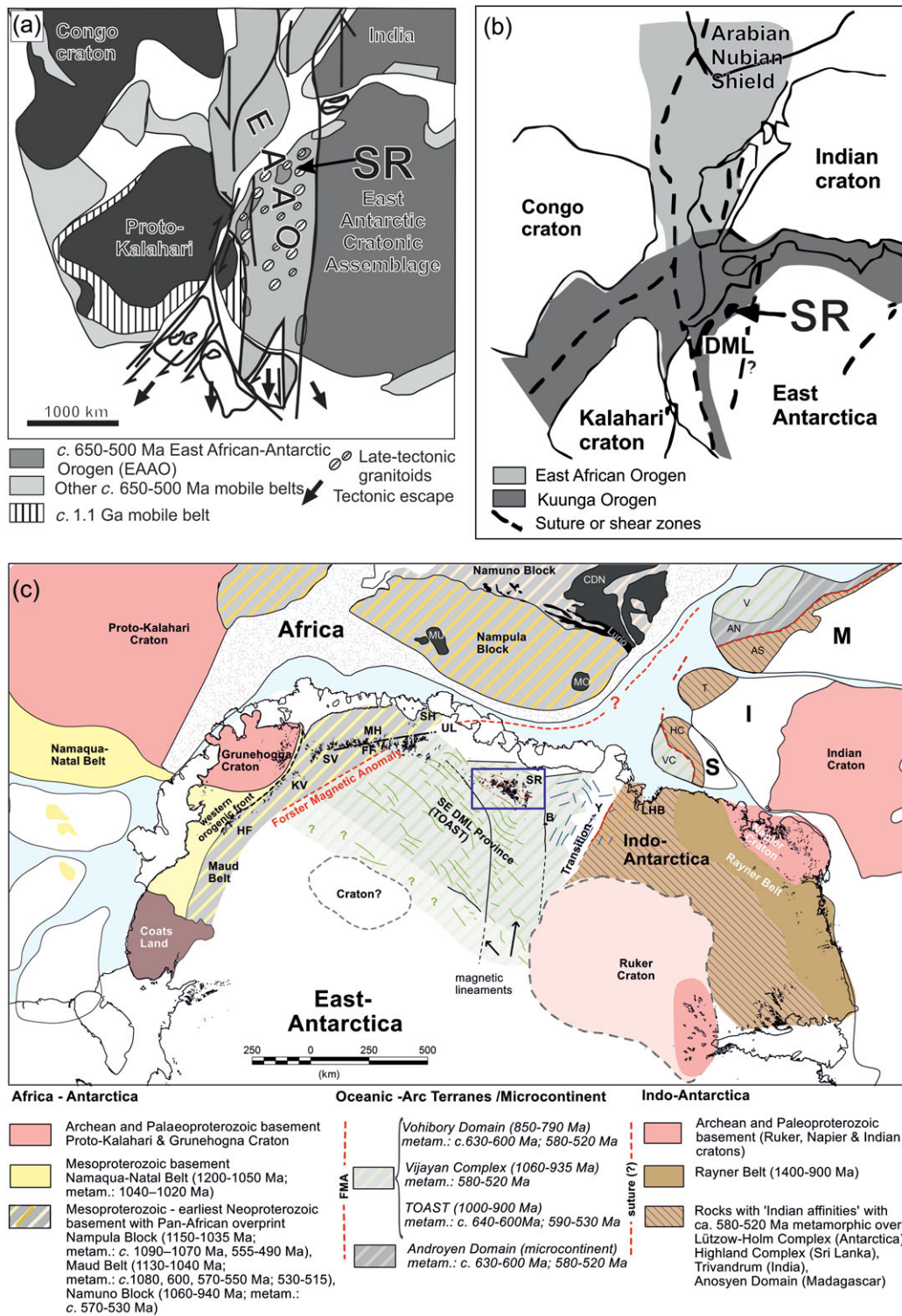
Fig. 1. (Colour online) Study area (SR, box in (c)) within Gondwana at *c.* 500 Ma located in (a) the eastern part of the EAAO after Jacobs & Thomas (2004) or (b) in the Kuunga Orogen after Meert (2003). (c) Major crustal fragments within East Antarctica are outlined based on combined geological and geophysical interpretation (e.g. Jacobs & Thomas, 2004; Riedel *et al.* 2013; Mieth & Jokat, 2014; Jacobs *et al.* 2015; Golynsky *et al.* 2018; Ruppel *et al.* 2018). Antarctica is shown in polar stereographic projection; major complexes and/or blocks within Africa (e.g. Macey *et al.* 2013) and Sri Lanka, India and Madagascar (e.g. Boger *et al.* 2015) are shown schematically. Boundaries of the TOAST are inferred from aeromagnetic data (Riedel *et al.* 2013; Ruppel *et al.* 2018), whereas the continuation of a possible suture in Sri Lanka, India and Madagaskar is adapted from Boger *et al.* (2015). AN – Androyen domain; AS – Anosyen domain; B – Belgica Mountains; C – Coats Land; CDN – Cabo Delgado Nappe Complex; FF – Filchnerfjella; H – Heimefrontfjella; HC – Highland Complex; I – India; KV – Kirwanveggen; S – Sri Lanka; SH – Schirmacher Hills; SR – Sør Rondane; SV – Sverdrupfjella; T – Trivandrum; LHB – Lützow–Holm Bay; M – Madagascar; MH - Mühlig-Hofmanng Gebirge; MO – Monapo Klippe; MU – Mugeba Klippe; U – Ulvetanna Lineament; V – Vohibory domain; VJ – Vijayan complex; Y – Yamato Mountains.
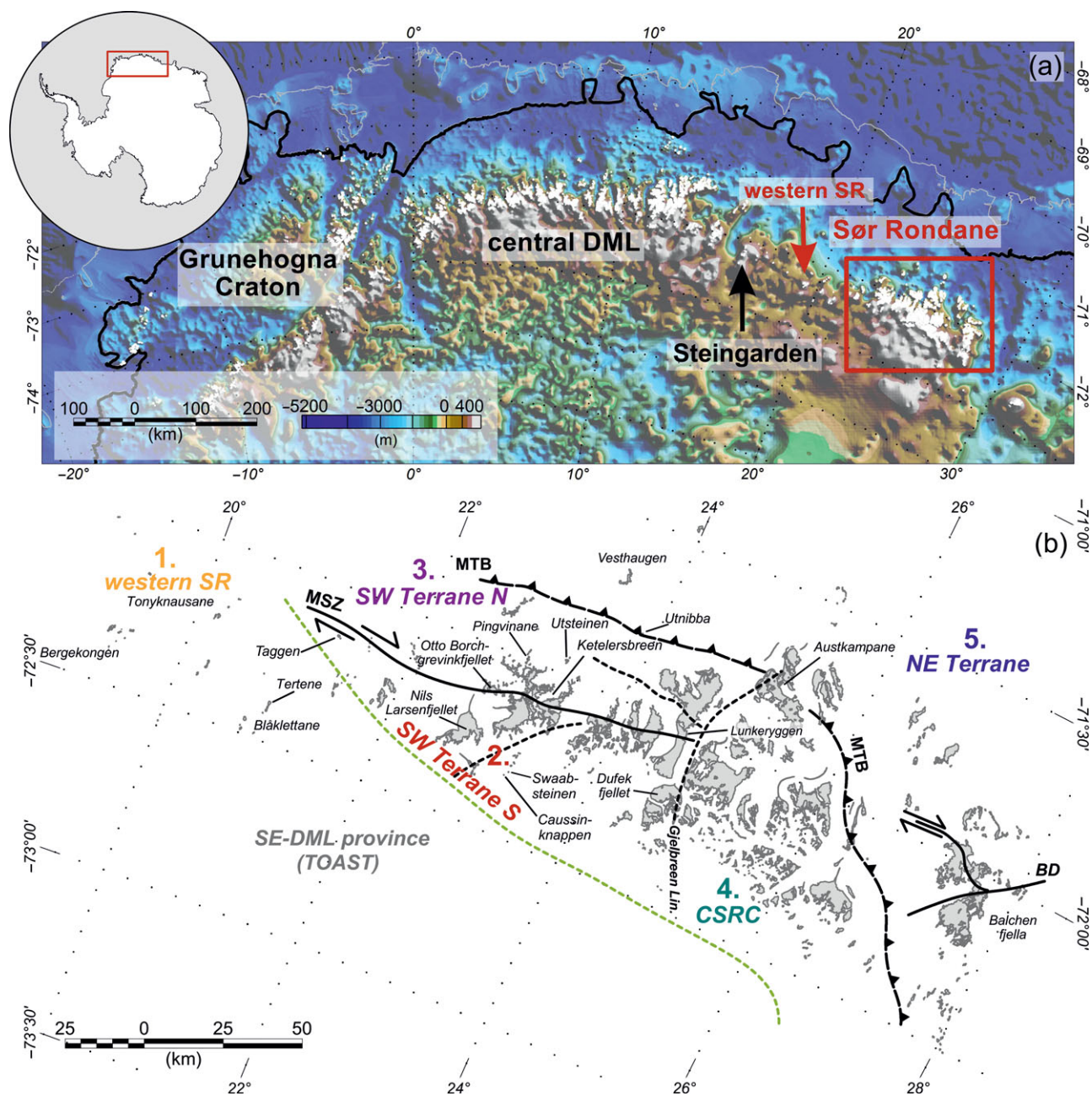
Fig. 2. (Colour online) Study area in East Antarctica. (a) Subsurface topography of Dronning Maud Land (DML) with study area in red (Bedmap2, Fretwell *et al.* 2013). (b) Exposed rocks (grey) and subdivision of Sør Rondane into five distinct tectonic domains. Boundaries are from Mieth *et al.* (2014). BD – Balchen detachment; CSCR – central Sør Rondane corridor; MSZ – Main Shear Zone; MTB – Main Tectonic Boundary; SR – Sør Rondane.

amalgamation of Gondwana. K–Ar and ^{40}Ar/^{39}Ar (short Ar/Ar) whole-rock and biotite ages from igneous and metamorphic rocks of eastern Sør Rondane of *c.* 490–420 Ma were interpreted to indicate cooling following the latest metamorphic event (Takigami *et al.* 1987; Takahashi *et al.* 1990; Takigami & Funaki, 1991; Osanai *et al.* 2013).

Recent geological and geophysical studies have provided insights into the Meso- to early Neoproterozoic history of the region (Hokada *et al.* 2013; Elburg *et al.* 2015; Jacobs *et al.* 2015; Ruppel *et al.* 2018), the intrusive activity during Gondwana assembly (Elburg *et al.* 2016), the structural and tectonic framework (Osanai *et al.* 2013; Owada *et al.* 2013; Mieth *et al.* 2014; Ruppel *et al.* 2015) and the Gondwana

disintegration (Krohne, 2017). To better understand the final assembly of Gondwana during the late Neoproterozoic – early Palaeozoic, we investigated the late-tectonic igneous and cooling history of a broad suite of samples from the Sør Rondane region to trace the geodynamic evolution during and after the formation of the EAAO across DML. In addition, we aim to test the hypothesis of collage-style accretion tectonics of the TOAST (Jacobs *et al.* 2015; Elburg *et al.* 2016). We present Ar/Ar ages from five distinct terranes of Sør Rondane, including the little-studied region between Sør Rondane and central DML (western SR), and the remote eastern areas of Sør Rondane (Fig. 2). In addition, new U–Pb zircon ages from syn- to post-tectonic granitoids constrain the timing of deformation along the Main Shear Zone (MSZ), the

boundary between the northern and southern parts of the SW Terrane of Sør Rondane (SW Terrane N and SW Terrane S, respectively).

2. Geological background and previous Rb–Sr, K–Ar and Ar/Ar thermochronology of Sør Rondane

Sør Rondane's late Mesoproterozoic – early Neoproterozoic (c. 1100–900 Ma) juvenile basement rocks lack significant remnants of Archaean or Palaeoproterozoic continental crust. Since late Mesoproterozoic time, the region has undergone oceanic arc and/or terrane accretion, probably related to tectonics outboard of Rodinia (e.g. Shiraishi et al. 2008; Jacobs et al. 2015; Elburg et al. 2016). The spatial extent of this so-called Tonian Oceanic Arc Super Terrane (TOAST) was estimated as c. 500 000 km^2, including the area to the south and SE of central DML and Sør Rondane; it likely continues to the Belgica Mountains (Fig. 1; Takigami & Funaki, 1991; Ruppel et al. 2018). The TOAST experienced medium- to high-grade metamorphism from c. 650 to 580 Ma, resulting from ocean closure and the final amalgamation of Gondwana. There is only minor evidence for Tonian metamorphism in the rocks of the TOAST (Jacobs, et al. 2017).

The SW Terrane S and a few scattered nunataks to the west represent the type locality of the TOAST (Fig. 2; Jacobs et al. 2017). It consists mainly of a gabbro–tonalite–trondhjemite–granodiorite complex (GTTG), dated at c. 1000–900 Ma; Nd whole-rock and Hf-in-zircon isotopic signatures indicate that this complex represents a juvenile oceanic arc (Kamei et al. 2013; Elburg et al. 2015). The Main Shear Zone delimits the SW Terrane S from the SW Terrane N (Fig. 2b); the latter is dominated by greenschist- to granulite-facies metasedimentary and meta-igneous rocks, with the youngest detrital zircon ages of c. 700 Ma (Otsuji et al. 2013; Owada et al. 2013). Peak metamorphic conditions, part of an anticlockwise pressure–temperature (P-T) path, were dated at c. 640–600 Ma (Adachi et al. 2013; Osanai et al. 2013).

To the NE, the SW Terrane is separated from the amphibolite- to granulite-facies metamorphic NE Terrane by the Main Tectonic Boundary (MTB) (Fig. 2b; Osanai et al. 2013). The NE Terrane comprises metasupracrustal rocks with the youngest detrital zircon ages at c. 750 Ma; metamorphism followed a clockwise P-T path and peaked at c. 640–600 Ma (Shiraishi et al. 2008). The two contrasting P-T paths on either side of the MTB were interpreted to result from thrusting of the NE Terrane over the SW Terrane during the Pan-African Orogeny (Adachi et al. 2013; Osanai et al. 2013). The former Sør Rondane Suture is interpreted here as part of the frontal thrust zone of the MTB rather than a suture zone between the NE and SW Terranes. So far, pre-750 Ma basement has not been recognized in the NE Terrane; it therefore remains unclear whether the NE Terrane is part of the TOAST or is a separate tectonic domain.

Intrusive rocks record at least four thermal pulses between c. 650 and 500 Ma in Sør Rondane, suggesting protracted accretion and collision in this part of the EAAO (e.g. Elburg et al. 2016). One particular igneous group is represented by granites of the Vengen type (Vengen: locality name) of age c. 560 Ma. They intruded along the MSZ and are weakly foliated, indicating a late syn- to post-tectonic emplacement (Shiraishi et al. 2008; Ruppel et al. 2015; Elburg et al. 2016). Metamorphic U–Pb zircon ages of c. 590–530 Ma were reported across the entire region and interpreted as recording post-collisional retrograde metamorphism and/or hydration after peak amphibolite-facies metamorphism

at c. 590–570 Ma (Shiraishi et al. 2008; Osanai et al. 2013; Elburg et al. 2016).

Previous Rb–Sr, K–Ar and Ar/Ar thermochronology data span c. 660–420 Ma (Osanai et al. 2013 and references therein). The distribution of K–Ar and Ar/Ar data shows an age trend across Sør Rondane, generally becoming younger from south to north. The oldest K–Ar cooling age of c. 660 Ma is from a gneiss from Nils Larsenfjellet in the SW Terrane S. Most K–Ar and Ar/Ar data scatter between 500 and 480 Ma and are from granitic and syenitic rocks at Lunkeryggen and a gneiss at Otto Borchgrevinkfjellet. The SW Terrane N provided one K–Ar biotite age of c. 500 Ma at Pingvinane (Takigami & Funaki, 1991). Rb–Sr cooling ages of c. 510–460 Ma are from granites and a gneiss collected from the central Sør Rondane corridor (CSRC, Fig. 2) (Deutsch et al. 1961; Pasteels & Deutsch, 1963). The NE Terrane yielded the youngest cooling ages: K–Ar biotite ages of c. 470 Ma at Austkampane; and K–Ar whole-rock ages of 430–420 Ma and K–Ar and Ar/Ar biotite ages of 490–440 Ma at Utnibba (Takigami et al. 1987). Osanai et al. (2013) interpreted the majority of the Rb–Sr, K–Ar and Ar/Ar ages within a range of c. 490–420 Ma as cooling ages, post-dating metamorphism.

Mieth et al. (2014) suggested a refinement of the tectonic subdivision of Sør Rondane by integrating new aeromagnetic data with the geological framework. The general subdivision into the NE and SW Terranes remained, whereas major lineaments were confirmed or redefined (e.g. MSZ, MTB, Sør Rondane Suture). The magnetic anomaly pattern prompted a subdivision of the SW Terrane S into a western, more tholeiitic, and an eastern, more calc-alkaline, portion of the GTTG complex (Kamei et al. 2013; Mieth et al. 2014). Furthermore, the CSRC, which is also characterized by more enriched Hf-isotopic signatures (Elburg et al. 2016), was introduced as a distinct tectonic domain, separating Sør Rondane in an eastern and western part (Fig. 2b). The CSRC was interpreted as being related to late Pan-African extensional tectonics (Mieth et al. 2014).

3. Samples and methods

3.a. Samples

In total, 28 new samples were analysed, including 25 samples for Ar/Ar (biotite and amphible) and 3 for U–Pb zircon dating (see Section 4.b below). Samples were collected during the 'Geodynamic Evolution of East Antarctica' (GEA) expeditions I and II in the austral summers of 2010/2011 and 2011/2012. They represent all major terranes and/or units previously identified by integrated geological–aerogeophysical studies. From SW to NE, our sampling for Ar/Ar dating included the following (Fig. 3).

(1) Six samples from scattered nunataks west of Sør Rondane in the magnetically distinct SE-DML province; one is from a moraine (J1221D_1). These samples include Stenian–Tonian GTTGs (J1211B_2, J1221D_1), Ediacarian–Cambrian garnet-bearing migmatites and orthogneiss sheets (J1211B_1, J1213C, J1213D) and a late- to post-tectonic granitoid (J1212C). The Ar/Ar dating used samples previously dated by the U–Pb zircon method (Jacobs et al. 2015).

(2) Ten samples from the SW Terrane S. We mainly sampled in the vicinity of the MSZ within the GTTG complex. The lithologies include mylonitic rocks of tonalitic composition (27C_1, 1208A1, 1203A4), gneisses (1131A1, 1131A2, 27 A_1, J1214_A2), biotite and amphibole schist (1205A2, 1218A1) and a late- to post-tectonic granitoid (1130D_1).
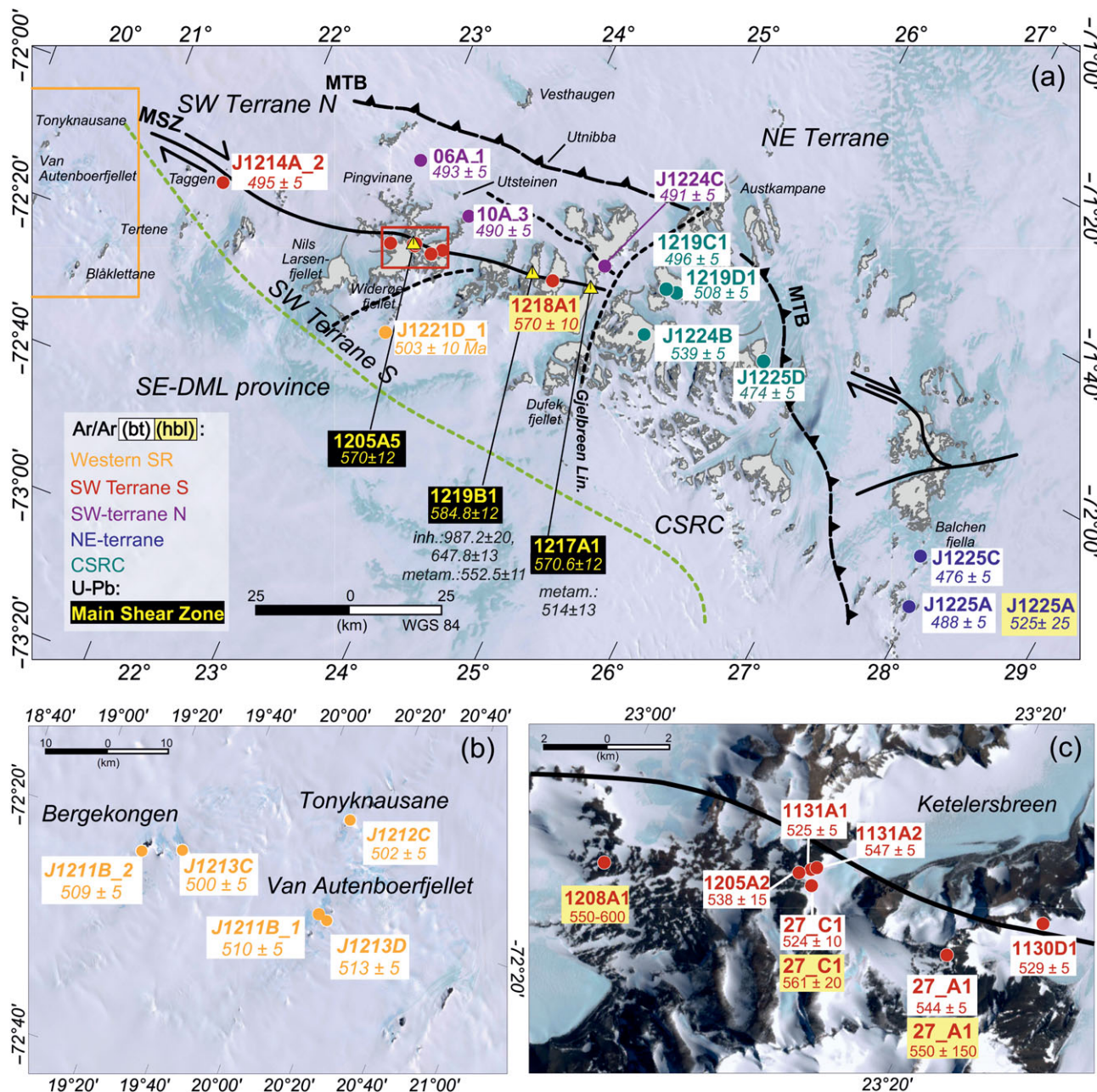
Fig. 3. (Colour online) Overview of the new $^{40}Ar/^{39}Ar$ and U–Pb age data. Localities with sample number and corresponding geochronological ages in millions of years (Ma). Colours refer to samples taken within distinct terranes. J1221D-1, a moraine sample, probably originated from the south, the western Sør Rondane (SE-DML province). (a) $^{40}Ar/^{39}Ar$ cooling ages are indicated by white background for biotite and yellow for hornblende; U–Pb zircon ages have a black background. Orange rectangle indicates the region of the samples from western Sør Rondane, shown in detail in (b). A close-up of the region along the MSZ is marked with the red rectangle and is illustrated in detail in (c). CSCR – central Sør Rondane corridor; MSZ – Main Shear Zone; MTB – Main Tectonic Boundary; SR – Sør Rondane.

(3) Three samples from the SW Terrane N, north of the MSZ, comprising an orthogneiss (06 A-1), a granitic gneiss (J1224C) and a metavolcanic rock (10A3).

(4) Four samples from the CSRC, including two gneisses (1219C1, 1219D1), a biotite-sillimanite-gneiss (J1224B) and a late- to post-tectonic granitoid from the easternmost CSRC (J1225D).

(5) Two samples from the easternmost NE Terrane, comprising a migmatic gneiss (J1225C) and a diorite (J1225A).

3.b. $^{40}Ar/^{39}Ar$ analyses

Ar/Ar analyses were carried out at the Argonlab Freiberg, TU Bergakademie Freiberg, Germany. Mineral processing used the electical-discharge SELFRAG® facility that yields grain sizes corresponding closely to the true crystal size; it also minimizes the proportion of broken grains (Sperner *et al.* 2014). We used the largest grain-size fraction from which it was possible to hand-pick optically inclusion-free crystals. The mineral separates were washed repeatedly in deionized water using an ultrasonic bath. After drying, the mineral separates were wrapped in Al foil and loaded into wells on Al discs (33 mm diameter) for irradiation. Irradiation was carried out for 3.8 hours without Cd-shielding at the LVR-15 research reactor of the Nuclear Research Institute in Řež, Czech Republic. The thermal neutron fluence was in the order of 6×10^{13} neutrons per (cm^2 s) at a thermal to fast neutron ratio of *c.* 1.1 (*c.* 7.6 MW reactor power; for detailed irradiation geometry

and reactor specifics see Rutte et al. 2015). Irradiated micas were unwrapped and loaded into 3×1 mm (diameter × depth) wells on oxygen-free copper discs (30 samples per disc). Hornblende separates were loaded into Mo-crucibles for furnace degassing. Stepwise heating of micas was performed using a power-controlled, floating, 30 W New Wave CO_2 laser system, with a defocused beam with a 3 mm diameter. The heating time was 5 minutes per step. Stepwise heating of hornblende separates was performed using a Createc high-temperature cell (HTC; for details see Pfänder et al. 2014), with a heating time of 10 minutes per step. Two GP50 getter pumps, one at room temperature and one at 400 °C, achieved gas purification. Cleaning time per step was 5 minutes for laser degassing and 10 minutes for furnace degassing. Argon isotope compositions were measured in static mode on a GV Instruments ARGUS noble gas mass spectrometer equipped with five Faraday cups, and 10^{12} Ohm resistors on mass positions 36–39 and a 10^{11} Ohm resistor on mass position 40. Typical blank levels were 2.5×10^{-16} mol ^{40}Ar and 8.1×10^{-18} mol ^{36}Ar. Measurement time was 7.5 minutes per step, acquiring 45 scans at 10 seconds integration time each. Mass bias was corrected assuming linear mass-dependent fractionation and using an atmospheric $^{40}Ar/^{36}Ar$ ratio of 298.6 ± 0.3 (Lee et al. 2006; Mark et al. 2011). For raw data reduction and time-zero intercept calculation, we used a Matlab® toolbox developed in-house. Inverse isochron and weighted mean ages were calculated using ISOPLOT 4.15 (Ludwig, 2008). All ages were calculated using Drachenfels sanidine (DRF1) as fluence monitor (25.682 ± 0.030 Ma). This in-house standard was calibrated against Fish Canyon Tuff sanidine, applying an age of 28.305 ± 0.036 Ma and using the decay constants given in Renne et al. (2010). Interference correction factors are given in online Supplementary Table S1 (available at http://journals.cambridge.org/geo) along with the raw data of the Ar isotope measurements. Ar/Ar age spectra and inverse isochron diagrams of all analysed samples are provided in online Supplementary Figure S1.

3.c. U–Pb zircon analyses

Zircon concentrates were separated from 1–2 kg sample material using standard methods. The final selection of the zircon grains for U–Pb dating was achieved by hand-picking under a binocular microscope. Zircon grains of all sizes and morphological types were selected, mounted in resin, and polished to approximately half their diameters. Zircons were analysed for U, Th and Pb isotopes by laser ablation inductively coupled plasma mass spectrometry (LA-ICP-MS) using a Thermo-Scientific Element 2 XR sector field ICP-MS coupled to a NewWave UP-193 Excimer Laser System at the Senckenberg Naturhistorische Sammlungen Dresden, Germany. Cathodoluminescence imagery guided the selection of the analysed spots and was used to study the zircon textures, aiding the interpretation of their geological history (e.g. Corfu et al. 2003). A teardrop-shaped, low-volume laser cell constructed by Ben Jähne (Dresden) and Axel Gerdes (Frankfurt am Main) was used to enable sequential sampling of heterogeneous grains (e.g. growth zones) during time-resolved data acquisition. Each analysis consisted of approximately 15 seconds background acquisition followed by 30 seconds of data acquisition, using a laser spot size of 25 or 35 µm. A common-Pb correction, based on the interference-corrected and background-corrected ^{204}Pb signal and a model Pb composition (Stacey & Kramers, 1975), was applied if necessary (i.e. if the corrected $^{207}Pb/^{206}Pb$ lay outside of the internal errors of the measured ratios). Raw data were corrected for

background signal, common Pb, laser-induced elemental fractionation, instrumental mass discrimination and time-dependent elemental fractionation of Pb/Th and Pb/U using an Excel® spreadsheet program developed by Axel Gerdes. Reported uncertainties were propagated by quadratic addition of the external reproducibility obtained from the standard zircon GJ-1 (c. 0.6 and 0.5–1.0% for $^{207}Pb/^{206}Pb$ and $^{206}Pb/^{238}U$, respectively) during individual analytical sessions, and the within-run precision of each analysis. Concordia diagrams (2σ error ellipses) and concordia and weighted mean ages (95% confidence level) were calculated using ISOPLOT 4.15 (Ludwig, 2012). To ensure reproducibility of the reference material, we report all calculated 2σ crystallization-age uncertainties < 2% as 2% in parentheses. For further details on the analytical protocol and data processing, see Gerdes & Zeh (2006) and Frei & Gerdes (2009). Cathodoluminescence images are provided in online Supplementary Figure S2 (available at http://journals.cambridge.org/geo) and the complete LA-ICP-MS zircon data are presented in online Supplementary Table S2.

4. Results

4.a. Ar/Ar dating of biotite and amphibole

The results are presented and described in regional order from SW to NE and grouped according to their geographic position within the distinct terranes (online Supplementary Fig. S1, available at http://journals.cambridge.org/geo). Table 1 summarizes the analytical results. In many samples, most of the steps are highly radiogenic (%$^{40}Ar^* > 99$); most data points therefore cluster close to the $^{39}Ar/^{40}Ar$ axis in the inverse isochron plots and provide poor fits to the $^{36}Ar/^{40}Ar$ versus $^{39}Ar/^{40}Ar$ data. Most biotite separates yielded flat sections in the age versus cumulative ^{39}Ar diagrams, with weighted mean ages (WMA) with mean square of weighted deviates (MSWD) around 1 and probabilities of fit > 5%; however, the amphibole spectra are commonly U-shaped and do not permit the calculation of a WMA for the majority of analyses. Our preferred age interpretation includes age uncertainties of $\pm 2\sigma$ and ≥ 1% of the age to account for sample complexities, in particular, the uncertainities in the calculated initial $^{40}Ar/^{36}Ar$.

4.a.1. Western Sør Rondane
4.a.1.1. J1211B_1, biotite, garnet–migmatite, Bergekongen (72.406267° S; 20.920250° E). This garnet-bearing migmatite from Bergekongen consists of quartz, K-feldspar, plagioclase and biotite. In a previous study, zircon cores of this sample were U–Pb zircon-dated at c. 1000 Ma, whereas zircon rims gave a $^{206}Pb/^{238}U$ concordia age of 546 ± 3 Ma (MSWD = 1.83) with the latter interpreted to date a metamorphic overprint (Jacobs et al. 2015). A total of 82.5% of the released ^{39}Ar provides an Ar/Ar biotite WMA of 510.9 ± 1.1 Ma (MSWD = 0.16); the inverse isochron age (IIA) at 510.5 ± 2.2 Ma (MSWD = 0.72) is identical, with an imprecise initial $^{40}Ar/^{36}Ar$ value of 450 ± 170, reflecting the high radiogenic yield. Our age interpretation is 510 ± 5 Ma.

4.a.1.2. J1213C, biotite, pegmatite gneiss, Bergtussen (72.337533° S; 19.472300° E). This coarse-grained pegmatite, intruding a migmatic gneiss from Bergtussen, shows moderate deformation; it consists mainly of quartz, plagioclase, K-feldspar and biotite. Zircons yielded a $^{206}Pb/^{238}U$ concordia age of 597 ± 7 Ma (MSWD = 3.13), interpreted as the crystallization

Table 1. $^{40}Ar/^{39}Ar$ ages. ALF – Argon Lab Freiberg; CSRC – central Sør Rondane corridor; IIA – inverse isochron age; MSWD – mean square weighted deviation; MSZ – Main Shear Zone; WMA – weighted mean ages

Sample	ALF device	Mineral	Weight (mg)	Grain size (μm)	WMA[a,b] ± 1σ (Ma)	MSWD (WMA)	IIA[b] ± 1σ (Ma)	MSWD (IIA)	$(^{40}Ar/^{36}Ar)_i$ (IIA)	%^{39}Ar	Steps (total)	Age interpretation (±2σ and ≥1%) (Ma)	Location
J1211_B1	Laser	Biotite	2.97	250–500	510.9 ± 1.1	0.16	510.5 ± 2.2	0.72	450 ± 170	82.5	5–19 (19)	510 ± 5	Western Sør Rondane
J1213C	Laser	Biotite	2.72	250–500	501.8 ± 1.3	1.20	499.3 ± 2.7	0.71	943 ± 290	87.4	6–21 (21)	500 ± 5	
J1211B_2	Laser	Biotite	2.23	250–500	509.6 ± 1.6	0.55	508.2 ± 2.8	1.6	409 ± 45	71.8	7–16 (18)	509 ± 5	
J1213D	Laser	Biotite	2.76	250–500	513.0 ± 1.0	0.74	–[c]			91.5	5–20 (20)	513 ± 5	
J1212C	Laser	Biotite	2.72	160–250	502.7 ± 1.0	1.03	500.2 ± 4.6	0.69	1476 ± 910	75.2	6–21 (21)	501 ± 5	
J1221D_1	Laser	Biotite	2.78	250–500	505.3 ± 1.5	0.86	501.8 ± 4.7	2.3	904 ± 440	80.4	6–19 (20)	503 ± 10	Moraine
1205A2	Laser	Biotite	2.24	80–250	542.7 ± 1.2	0.86	535.5 ± 8.2	0.59	987 ± 490	70.8	7–16(16)	538 ± 15	SW Terrane S, affected by MSZ
27C_1	Laser	Amphibole	2.25	80–250	561.5 ± 2.8	0.25	560.2 ± 4.1	1.6	8349 ± 5500	96.4	4–5 (5)	561 ± 20	
27C_1	Laser	Biotite	2.72	80–250	534.6 ± 3.3	4.1	523.2 ± 4.1	1.07	1145 ± 230	56.3	8–18 (20)	524 ± 10	
1131A1	Laser	Biotite	2.23	160–250	526.0 ± 1.3	0.77	522.0 ± 6.3	1.5	900 ± 470	78.3	6–18 (18)	525 ± 5	
1131A2	Laser	Biotite	2.24	160–250	547.4 ± 1.7	0.29	548.1 ± 3.3	3.3	287 ± 110	80.5	6–18 (18)	547 ± 5	
27 A_1	Furnace	Amphibole	40.46	80–250	–[c]		550 ± 75	0.50	8349 ± 5500	30	12–15 (18)	550 ± 150	
27 A_1	Laser	Biotite	2.25	80–250	543.4 ± 1.2	0.08	543.9 ± 2.7	0.81	332 ± 170	68.7	7–17 (17)	544 ± 5	
1130D1	Laser	Biotite	2.25	80–160	528.9 ± 1.3	0.07	528.4 ± 4.4	0.17	617 ± 490	84.9	6–18 (18)	529 ± 5	
1218A1	Furnace	Amphibole	29.44	<160–250	571.1 ± 1.6	1.5	570.2 ± 2.6	0.20	320 ± 17	19.6	15–18 (18)	570 ± 20	
1203A4	Furnace	Amphibole	40.97	<160	–[c]		605 ± 300	1.11	40768 ± 7800	47	8–15 (20)	?≤600	
1208A1	Furnace	Amphibole	28.97	<160–250	–[c]		–[c]					550–600	
J1214A_2	Laser	Biotite	2.71	80–250	494.9 ± 1.1	0.77	493 ± 12	2.6	643 ± 420	80.3	7–20 (20)	495 ± 5	SW Terrane S, reset?
06 A_1	Laser	Biotite	2.30	80–250	493.4 ± 1.2	0.49	491.5 ± 7.4	2.6	660 ± 420	81.9	11–26 (26)	493 ± 5	SW Terrane N
10 A_3	Laser	Biotite	2.22	80–250	490.4 ± 1.5	0.54	–[c]			92.1	6–19 (19)	490 ± 5	
J1224C	Laser	Biotite	2.74	80–250	491.2 ± 1.1	0.38	–[c]			76.8	6–20 (20)	491 ± 5	
J1224B	Laser	Biotite	2.73	80–250	538.3 ± 1.2	0.04	539.0 ± 2.1	0.39	283 ± 63	90.9	7–22 (22)	539 ± 5	CSRC, affected by MSZ?
1219C1	Laser	Biotite	2.26	160–250	497.7 ± 1.1	0.47	494.9 ± 2.9	1.17	455 ± 100	57.3	7–15 (17)	496 ± 5	CSRC
1219D1	Laser	Biotite	2.21	80–250	508.4 ± 1.6	0.79	505.3 ± 4.5	10.8	378 ± 100	66.7	9–15 (15)	508 ± 5	
J1225D	Laser	Biotite	2.26	250–500	475.1 ± 1.0	0.38	473.5 ± 2.5	0.64	665 ± 320	74.7	6–20 (20)	474 ± 5	
J1225A	Furnace	Amphibole	24.17	160–250	–[c]		525 ± 12	0.24	7295 ± 12000	80.5	9–19 (21)	525 ± 25	NE Terrane
J1225A	Furnace	Amphibole	24.17	160–250	–[c]		499.9 ± 9.0	0.061	350 ± 12	1.1	1–4 (21)	500 ± 20	
J1225A	Laser	Biotite	2.73	250–500	487.6 ± 1.5	0.30	488.0 ± 2.8	2.5	365 ± 71	98.2	5–21 (21)	488 ± 5	
J1225C	Laser	Biotite	2.24	80–250	476.8 ± 1.1	0.85	475.9 ± 5.0	6.5	462 ± 270	85.1	6–20 (21)	476 ± 5	

[a]Calculated by weighting each age analysis by its reciprocal variance.
[b]Based on fraction of ^{39}Ar and steps listed.
[c]No meaningful calculation possible.

age of the pegmatite (Jacobs *et al.* 2015). A total of 87.4% of the released ^{39}Ar yielded an Ar/Ar biotite WMA of 501.8 ± 1.3 Ma (MSWD = 1.2) and an IIA of 499.3 ± 2.7 Ma (MSWD = 0.71), the latter with an imprecise, non-atmospheric initial ^{40}Ar/^{36}Ar value of 943 ± 290. Our age interpretation is 500 ± 5 Ma.

4.a.1.3. J1211B_2, biotite, metagabbro/enderbite, Bergekongen (72.358167° S; 19.288833° E).
This metamorphic rock is mainly composed of plagioclase and coarse-grained orthopyroxene. Biotite and amphibole formed during amphibolite-facies retrogression. Zircons provided a ^{206}Pb/^{238}U concordia age of 916 ± 13 Ma (MSWD = 1.85), interpreted as the crystallization age of the gabbro protolith (Jacobs *et al.* 2015). Biotite yielded a WMA of 509.6 ± 1.6 Ma (MSWD = 0.55) and an IIA of 508.2 ± 2.8 Ma (MSWD = 1.6), comprising 71.8% of the released ^{39}Ar; the initial ^{40}Ar/^{36}Ar value of 409 ± 45 indicates extraneous ^{40}Ar. The preferred age is 509 ± 5 Ma.

4.a.1.4. J1213D, biotite, pegmatitic granitoid, Van Autenboerfjellet (72.362983° S; 20.244717° E).
This pegmatite is from a coarse-grained granite sheet intruding into migmatic gneisses. The sample consists of quartz, plagioclase, K-feldspar and biotite. Zircons gave a ^{206}Pb/^{238}U concordia age of 582 ± 5 Ma (MSWD = 2.25), interpreted as the crystallization age (Jacobs *et al.* 2015). A total of 91.5% of the released ^{39}Ar yielded a biotite WMA of 513.0 ± 1.0 Ma (MSWD = 0.74); this sample did not allow an IIA calculation. The hump in the central part of the spectrum indicates that these steps incorporated minor extraneous Ar. Our preferred age is 513 ± 5 Ma.

4.a.1.5. J1212C, biotite, discordant granitic gneiss sheet, Tonyknausane (72.212600° S; 20.182767° E).
This granitic gneiss cuts meta-supracrustal gneisses, is mainly composed of quartz, plagioclase, K-feldspar, biotite and titanite. Quartz and feldspar show undulose extinction, and quartz also shows grain-boundary-migration recrystallization. Plagioclase has deformation twins and myrmekite; K-feldspar is altered. Dark brown biotite is idiomorphic to hypidiomorphic. The ^{206}Pb/^{238}U concordia zircon age of 528 ± 6 Ma (MSWD = 3.63) was interpreted as the crystallization age of the granitic protolith (Jacobs *et al.* 2015). The biotite WMA of 502.7 ± 1 Ma (MSWD = 1.03) and the IIA of 500.2 ± 4.6 Ma (MSWD = 0.69) include 75.2% of the released ^{39}Ar; the initial ^{40}Ar/^{36}Ar value of 1476 ± 910 relects the high radiogenic yield. Our preferred age is 501 ± 5 Ma.

4.a.1.6. Sample J1221D_1, biotite, grey gneiss, moraine sample (72.33105° S; 23.25415° E).
This gneiss from a moraine between Swaabsteinen and Causinknappen (Figs 2, 3) consists mainly of quartz, plagioclase, microcline, myrmekite and biotite. Quartz shows undulose extinction and subgrain-rotation and grain-boundary-migration recrystallization. Zircon cores provided a weighted mean ^{206}Pb/^{238}U age of 1087 ± 28 Ma (MSWD = 2.5), while metamorphic rims yielded a weighted mean ^{206}Pb/^{238} age of 542 ± 5 Ma (MSWD = 2.8) (Jacobs *et al.* 2017). Dark brown, columnar biotite shows no preferred orientation. A total of 80.4% of the released ^{39}Ar yielded a biotite WMA of 505.3 ± 1.5 Ma (MSWD = 0.86) and a IIA at 501.8 ± 4.7 Ma (MSWD = 2.3) with a ^{40}Ar/^{36}Ar value of 904 ± 440; this is consistent with the hump in the central part of the spectrum, which indicates that these steps incorporated extraneous Ar. Our preferred age is 503 ± 10 Ma.

4.a.2. SW Terrane S adjacent to the MSZ

4.a.2.1. Sample 1205A2, biotite, biotite schist, Dry Valley (72.10802° S; 23.18322° E).
This hornblende-biotite schist from the northern part of Dry Valley (Fig. 4a) consists of plagioclase, amphibole, chlorite, quartz, biotite, clinopyroxene and epidote. Quartz shows grain-boundary-migration recrystallization. Dark brown biotite and greenish-blue hornblende define the foliation. Accessories are epidote, titanite and rutile. A total of 70.8% of the released ^{39}Ar defines a biotite WMA of 542.7 ± 1.2 Ma (MSWD = 0.86); the IIA is 535.5 ± 8.2 Ma (MSWD = 0.59) with an ill-defined initial ^{40}Ar/^{36}Ar of 987 ± 490. The slightly hump-shaped spectrum indicates extraneous Ar. Our preferred age, 538 ± 15 Ma, emphasizes the younger age steps at the high-temperature degassing end of the spectrum.

4.a.2.2. Sample 27C_1, biotite and amphibole, mylonitic grano-diorite gneiss, Dry Valley (72.11° S; 23.1987° E).
This banded gneiss, composed of layers of recrystallized feldspar and quartz, was sampled at the western side of Ketelersbreen. Quartz shows both subgrain-rotation and grain-boundary-migration recrystallization. Plagioclase, K-feldspar and hornblende form porphyroclasts with asymmetric pressure-shadow tails of recrystallized quartz, hornblende and biotite. Dark brown biotite and greenish-blue hornblende occur within the foliation. Epidote and opaque minerals are accessories. A total of 56.3% of the released ^{39}Ar yielded a biotite WMA of 534.6 ± 3.3 Ma; the high MSWD of 4.1 reflects the hump-shape of the spectrum. The IIA of 523.2 ± 4.1 Ma (MSWD = 1.07) is younger with an initial ^{40}Ar/^{36}Ar value of 1145 ± 230. Our preferred age interpretation of 524 ± 10 Ma emphasizes the youngest high-temperature steps and follows the IIA. A total of 96.4% of the released ^{39}Ar yielded an amphibole WMA of 561.5 ± 2.8 Ma (MSWD = 0.25). This date is based on only two steps; the IIA of all five steps (the small amount of material did not allow more steps to be measured) at 560.2 ± 4.1 Ma (MSWD = 1.6; ^{40}Ar/^{36}Ar = 8349 ± 5500) may indicate that this date has geological meaning. Our preferred age is 561 ± 20 Ma.

4.a.2.3. Sample 1131A1, biotite, biotite schist, Ketelersbreen West (72.10577° S; 23.19255° E).
This fine-grained, foliated biotite schist is from west of Ketelersbreen close to the MSZ (Fig. 4b). Quartz occurs in bands as coarse-grained porphyroclasts and small recrystallized grains. Plagioclase porphyroclasts showing bulging recrystallization and strong sericitization are partly replaced by quartz, and record dextral shear sense by asymmetric, biotite-rich pressure-shadow tails. Biotite, chlorite and muscovite form the foliation. The mineral association, with quartz and plagioclase, and minor amounts of chlorite, biotite, muscovite and amphibole, suggests that this schist formed due to localized shearing of a tonalitic host rock under retrograde, greenschist-facies conditions. A total of 78.3% of the released ^{39}Ar yielded a biotite WMA of 526.0 ± 1.3 Ma (MSWD = 0.77) and an IIA of 522 ± 6.3 (MSWD = 1.5). Again, the high radiogenic yield results in an ill-defined initial ^{40}Ar/^{36}Ar value of 900 ± 470; the hump-shaped spectrum reflects the extraneous Ar in this sample. Our preferred age is 525 ± 5 Ma.

4.a.2.4. Sample 1131A2, biotite, mylonitic diorite gneiss, Ketelersbreen West (72.10470° S; 23.19660° E).
This mylonitized diorite is from the eastern side of Ketelersbreen. The chief constituent is plagioclase, which forms asymmetric porphyroclasts (Fig. 5a). Amphibole, chlorite and biotite form the foliation.

Fig. 4. (Colour online) Field photographs of samples collected along the Main Shear Zone (MSZ). (a) Dry Valley, mylonitic biotite schist (1205A2); (b) Ketelersbreen West, mylonitic diorite (1131A1); and (c) Gunnestadbreen West, mylonitic monzogranite (1130D1); (d, e) Ridge between Ellisbreen and Jenningsbreen, view towards the west along-strike of the MSZ and close-up of mylonitic rock with tonalitic composition at this location (1218A1).

Quartz shows grain-boundary-migration recrystallization and occurs in bands. A total of 80.5% of the released ^{39}Ar provided a biotite WMA of 547.4 ± 1.7 Ma (MSWD = 0.29) and an IIA of 548.1 ± 3.3 Ma (MSWD = 3.3; initial ^{40}Ar/^{36}Ar value = 287 ± 110). Our preferred age is 547 ± 5 Ma.

4.a.2.5. Sample 27 A_1, biotite and amphibole, mylonitic garnet–biotite–hornblende gneiss, Dry Valley (72.113° S; 23.340083° E). This gneiss from SE of Ketelersbreen consists of quartz, plagioclase and minor K-feldspar, biotite and amphibole. Quartz shows undulose extinction, subgrain-rotation and grain-boundary-migration recrystallization. The feldspars show bulging recrystallization. Dark brown biotite and greenish-blue hornblende parallel the foliation; biotite also occurs in the pressure-shadow tails of feldspar porphyroclasts. Accessory minerals are garnet, zircon, epidote and opaque minerals. A total of 68.7% of the released ^{39}Ar provided a biotite WMA of 543.4 ± 1.2 Ma (MSWD = 0.08) and an IIA of 543.9 ± 2.7 Ma (MSWD = 0.81; ^{40}Ar/^{36}Ar initial = 332 ± 170). Our preferred age is 544 ± 5 Ma. Amphibole of the same sample yielded a complex spectrum; the IIA, plagued by the high radiogenic yield, indicates an age of 550 ± 150 Ma, close to that of the biotite.

4.a.2.6. Sample 1130D1, biotite, mylonite of granitic composition, Gunnestadbreen West (72.09382° S; 23.41065° E). This mylonitic sample from the Vengen/Vikinghøgda granite was taken close to the MSZ. It contains quartz, plagioclase, and K-feldspar as major, and biotite, muscovite, chlorite, titanite and magnetite as minor components (Fig. 4c). Asymmetric plagioclase and K-feldspar porphyroclasts, indicating a dextral sense of shear, are surrounded by recrystallized plagioclase and bands of elongated quartz (Fig. 5b). Dark brown biotite occurs along the foliation and in the pressure shadows of plagioclase porphyroclasts. The Vengen/Vikinghøgda granitoids yielded crystallization ages of 562 ± 7 Ma (Shiraishi *et al.* 2008) and 551 ± 8 Ma (Elburg *et al.* 2016). A total of 84.9% of the released ^{39}Ar provided a biotite WMA of 528.9 ± 1.3 Ma (MSWD = 0.07) and a IIA of 528.4 ± 4.4 Ma (MSWD = 0.17; ^{40}Ar/^{36}Ar = 617 ± 490). Our preferred age is 529 ± 5 Ma.

4.a.2.7. Sample 1218A1, amphibole, mylonitic amphibole schist, ridge between Ellisbreen and Jenningsbreen (72.05343° S; 24.29992° E). This mylonite of tonalitic composition from a ridge between Ellisbreen and Jenningsbreen in the central part of the MSZ (Figs 4d, e) consists mainly of amphibole, plagioclase, quartz,
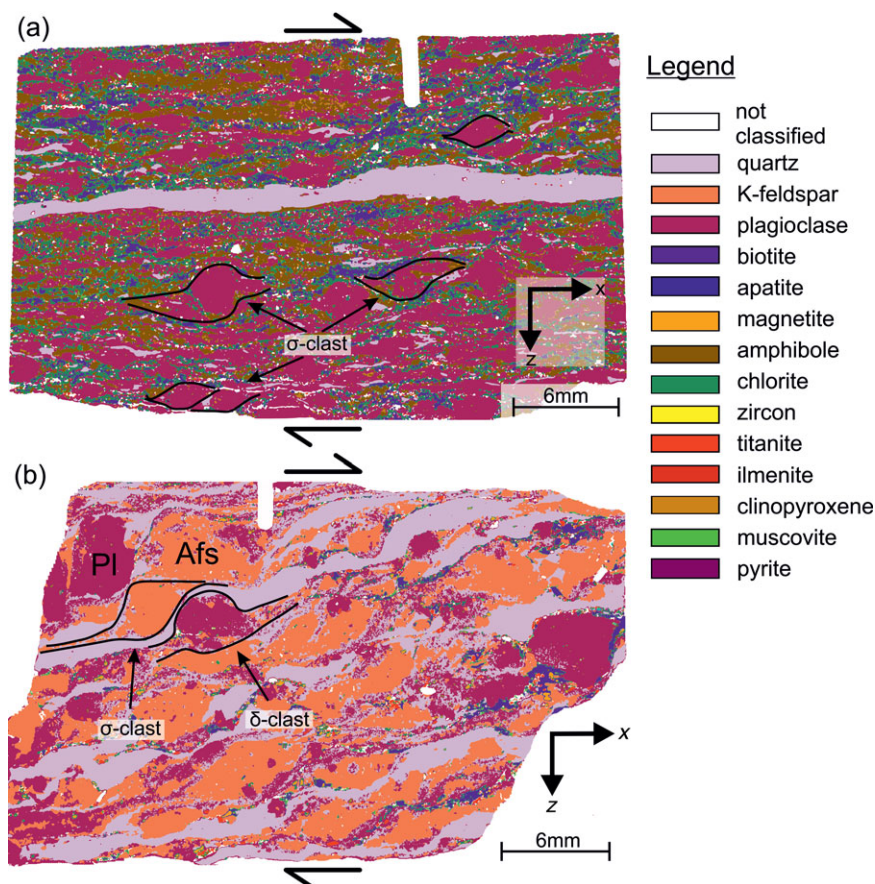
Fig. 5. (Colour online) Composition of rock samples used for ^{40}Ar/^{39}Ar dating located close to the MSZ. Rotated porphyroclasts whithin these thin sections indicate dextral shear. Thin sections were mapped with energy dispersive X-ray fluorescence with the M4 Tornado. (a) Sample 1130D1, mylonitic monzogranite; and (b) sample 1131A2, mylonitic rock of dioritic composition.

scapolite and clinopyroxene. Epidote, chlorite, clinozoisite, ilmenite, biotite, hornblende and magnetite are accessories. Quartz in bands is elongated and shows subgrain-rotation and grain-boundary-migration recrystallization. Relict plagioclase porphyroclasts are mostly recrystallized. Greenish-blue hornblende and fine-grained biotite define the foliation. Just 19.6% of the released ^{39}Ar define an amphibole WMA of 571.1 ± 1.6 Ma (MSWD = 1.5) and an IIA of 570.2 ± 2.6 Ma (MSWD = 0.2; initial ^{40}Ar/^{36}Ar = 320 ± 17). Our age interpretation is 570 ± 20 Ma.

4.a.2.8. Sample 1203A4, amphibole, orthomylonite of tonalitic composition, ridge west of Ellisbreen (72.0824° S, 23.0126° E). This mylonite consists mainly of foliation-parallel, greenish-blue hornblende, clinopyroxene, plagioclase and minor quartz. Plagioclase porphyroclasts are altered to clinozoisite and epidote. Accessory minerals are epidote, opaques and titanite. No meaningful age could be calculated for this sample; the isochron implies high amounts of extraneous Ar and an amphibole date likely younger than *c.* 600 Ma.

4.a.2.9. Sample 1208A1, amphibole, mylonite of tonalitic composition, Widerøfjellet West (72.12718° S; 23.0126° E). This mylonite from the western Dry Valley consists mainly of quartz, plagioclase, greenish-blue hornblende and dark brown biotite. Feldspar porphyroclasts have recrystallized mantles and asymmetric pressure shadows. Hornblende defines the foliation. Epidote is accessory. The amphibole yielded a complex spectrum, possibly a mixture

between atmosphere, radiogenic components and extraneous Ar; two four-point isochrons through different steps may define an amphibole age range of 550–600 Ma.

4.a.2.10. Sample J1214A_2, biotite, granitic gneiss, ridge east of Taggen (72.14513° S; 21.6089° E). This medium-grained orthogneiss contains quartz of variable grain size with undulose extinction and grain-boundary-migration recrystallization; recovery fabrics occur. Greenish-blue hornblende, K-feldspar and plagioclase are rare. Light- to dark-brown biotite with a columnar to radial texture is common and partly altered to chlorite. Accessories are zircon, epidote and opaques. U–Pb zircon dating yielded a crystallization age of 980 ± 8 Ma (MSWD = 2.74) (Jacobs *et al.* 2015). A total of 80.3% of the released ^{39}Ar provided a biotite WMA of 494.9 ± 1.1 Ma (MSWD = 0.77) and an IIA of 493 ± 12 Ma (MSWD = 2.6) with an imprecise initial ^{40}Ar/^{36}Ar value of 643 ± 420 due to the high radiogenic yield. Our preferred age is 495 ± 5 Ma.

4.a.3. SW Terrane N
4.a.3.1. Sample 06 A_1, biotite, orthogneiss, Fokknuten (71.9139°S; 22.97610° E). This grey orthogneiss consists of quartz, feldspar, biotite and hornblende. Quartz shows undulose extinction and grain-boundary-migration recrystallization. Plagioclase and microcline are common. Dark brown, columnar biotite and greenish-blue hornblende form the foliation. Accessory minerals are titanite, zircon and opaques. A total of 81.9% of the released ^{39}Ar

yielded a biotite WMA of 493.4 ± 1.2 Ma (MSWD = 0.49) and an IIA of 491.5 ± 7.4 Ma (MSWD = 2.6; initial ^{40}Ar/^{36}Ar = 660 ± 420). The weakly hump-shaped spectrum indicates extraneous Ar in the intermediate-temperature steps; WMAs and IIAs calculated for parts of the spectrum yielded identical ages. Our preferred age is 493 ± 5 Ma.

4.a.3.2. Sample 10 A_3, biotite, grey gneiss, Teltet (71.9924° S; 23.49375° E).
This gneiss is interpreted as a metavolcanic rock; it consists of coarse-grained quartz and plagioclase set in a finer-grained groundmass of quartz, feldspar and dark-brown biotite with accessory titanite. Calcite and muscovite are secondary minerals. A total of 92.1% of the released ^{39}Ar provided a biotite WMA of 490.4 ± 1.5 Ma (MSWD = 0.54); no IIA calculation was possible. Our preferred age is 490 ± 5 Ma.

4.a.3.3. Sample J1224C, biotite, granitic gneiss, Bratnipene South (71.96869° S; 24.26387° E).
This strongly foliated orthogneiss consists of quartz, feldspar and biotite with accessory allanite, titanite, apatite, zircon and opaques. Plagioclase is often saussuritized, and quartz sometimes forms bands. A total of 76.8% of the released ^{39}Ar yielded a biotite WMA of 491.2 ± 1.1 Ma (MSWD = 0.38); due to the high radiogenic yield, no meaningful IIA could be calculated. Our preferred age is 491 ± 5 Ma.

4.a.4. Central Sør Rondane corridor
4.a.4.1. Sample J1224B, biotite, biotite-sillimanite-gneiss, Mefjell (72.07886° S; 25.13041° E).
This fine- to medium-grained gneiss consists of plagioclase, quartz, olive-green biotite, sillimanite, plenty of magnetite and accessory apatite. A total of 90.9% of the released ^{39}Ar provided a biotite WMA of 538.3 ± 1.2 Ma (MSWD = 0.04) and an IIA of 539.0 ± 2.1 Ma (MSWD = 0.39; initial ^{40}Ar/^{36}Ar = 283 ± 63); our preferred age is 539 ± 5 Ma.

4.a.4.2. Sample 1219C1, biotite, garnet–biotite gneiss, Menipa (71.95688° S; 25.13605° E).
This banded gneiss at Menipa is mainly composed of K-feldspar, plagioclase, quartz, biotite and garnet. A total of 57.3% of the released ^{39}Ar yielded a biotite WMA of 497.7 ± 1.1 Ma (MSWD = 0.47) and an IIA of 494.9 ± 2.9 Ma (MSWD = 1.17) with an initial ^{40}Ar/^{36}Ar value of 455 ± 100. Our preferred age is 496 ± 5 Ma.

4.a.4.3. Sample 1219D1, biotite, garnet-sillimanite-biotite gneiss, Menipa (71.95467° S; 25.21993° E).
This gneiss consists of microcline, plagioclase, quartz and biotite with accessory sillimanite, garnet and titanite. A total of 66.7% of the released ^{39}Ar provided a biotite WMA of 508.4 ± 1.6 Ma (MSWD = 0.79). The IIA of 505.3 ± 4.5 Ma with an MSWD of 10.8 indicates the presence of non-analytical scatter given by the high radiogenic yield and reflected in the initial ^{40}Ar/^{36}Ar value of 378 ± 100. This sample also shows pronounced Ar loss in the low-temperature steps. Our preferred age is 508 ± 5 Ma.

4.a.4.4. Sample J1225D, biotite, granite, Bautaen, (72.01281° S; 26.06616° E).
This granite gave a weighted mean ^{206}Pb/^{238}U zircon age of 532 ± 3 Ma, interpreted to date its crystallization. It consists of quartz, plagioclase, microcline and myrmekite. Biotite is weakly altered to chlorite, and titanite is associated with opaques (Elburg *et al.* 2016). A total of 74.7% of the released ^{39}Ar yielded a biotite WMA of 475.1 ± 1.0 Ma (MSWD = 0.38) and an IIA of 473.5 ± 2.5 Ma (MSWD = 0.64); the initial ^{40}Ar/^{36}Ar value is

665 ± 320, again imprecise due to the high radiogenic yield. Our preferred age is 474 ± 5 Ma.

4.a.5. NE Terrane
4.a.5.1. Sample J1225A, biotite and amphibole, diorite, NE Terrane (72.38207° S; 27.97441° E).
This coarse-grained diorite consists mainly of plagioclase, dark brown biotite, hornblende and quartz. A total of 98.2% of the released ^{39}Ar provided a biotite WMA of 487.6 ± 1.5 Ma (MSWD = 0.30) and an IIA of 488.0 ± 2.8 Ma (MSWD = 2.5; initial ^{40}Ar/^{36}Ar value = 365 ± 71). Our preferred age is 488 ± 5 Ma. The amphibole spectrum is complex. IIAs at *c.* 534, 525 and 500 Ma for the high- to low-temperature steps can be calculated; the low-temperature IIA may represent an amphibole-biotite mixture (biotite inclusions in the amphibole).

4.a.5.2. Sample J1225C, biotite, migmatitic gneiss, NE Terrane (72.26139° S; 27.86756° E).
This coarse-grained gneiss consists of quartz, myrmekite, perthitic microcline, biotite and minor olive-green hornbende. Feldspars are dynamically recrystallized. A total of 85.1% of the released ^{39}Ar yielded a biotite WMA of 476.8 ± 1.1 Ma (MSWD = 0.85); the IIA is 475.9 ± 5.0 Ma (MSWD = 6.5; initial ^{40}Ar/^{36}Ar = 462 ± 270). Our preferred age is 476 ± 5 Ma.

4.b. U–Pb zircon ages
Zircon U–Pb data were acquired for two granitic dykes and one syenitic stock that crop out along the MSZ (Figs 6, 7, S2; Tables 2, S2).

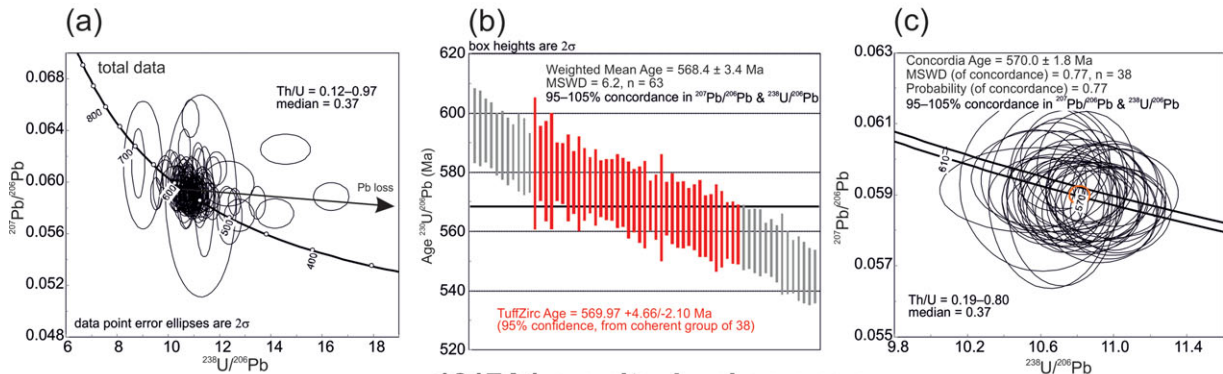### 4.b.1. Sample 1205A5, monzogranitic dyke, Dry Valley (72.10802° S; 23.18322° E)
This foliated dyke cross-cuts amphibolite- to greenschist-facies mylonites of the central MSZ (Fig. 7a) and is mainly composed of quartz, K-feldspar and plagioclase, with minor amounts of titanite and secondary scapolite and epidote. Quartz shows grain-boundary-migration recrystallization. K-feldspar is recrystallized and contains deformation twins. The large plagioclase grains show sericitization. The foliation is co-linear with the mylonitic foliation of the MSZ.

The sample contains small (up to 150 μm), mainly prismatic, euhedral zircons (online Supplementary Fig. S2a). A total of 106 spots were measured with 94 concordant analyses; the mostly younger, discordant analyses imply lead loss from *c.* 580 Ma (Fig. 6a). The 95–105% concordant spots yielded a population of normal distributed ages for which we obtained an age of 570 + 5/ − 2 Ma (coherent group of 38 out of 63 analyses) with the TuffZirc algorithm of Ludwig & Mundil (2002), which minimizes both positive (from xenocrysts or cores) and negative (from Pb loss) age biases (Fig. 6b). Most of the 38 analyses were conducted on oscillatory zoned zircon cores with sometimes weakly luminescent rims (online Supplementary Fig. S2a). These spots yielded a concordia age of 570.0 ± 1.8 (12) Ma (Fig. 6c). The Th/U ratios span 0.19–0.80 with a median of 0.37 typical for igneous origin. The concordia age of 570 ± 12 Ma is interpreted as the crystallization age of the monzogranitic dyke.
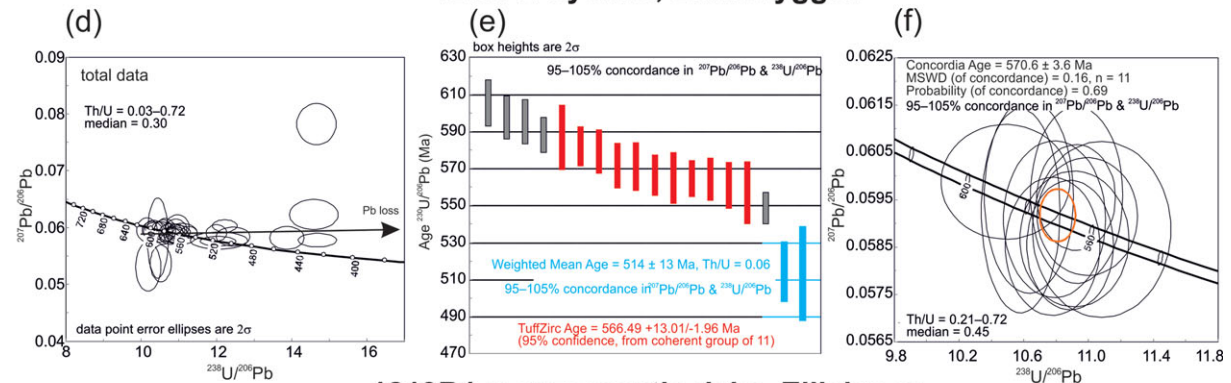
4.b.2. Sample 1217A1, syenite, Lunkeryggen E (72.03301° S; 24.59775° E)
This syenite is from the eastern flank of Lunkeryggen along the easternmost part of the known extent of the MSZ (Fig. 7b). The most common mineral – K-feldspar – shows oscillatory
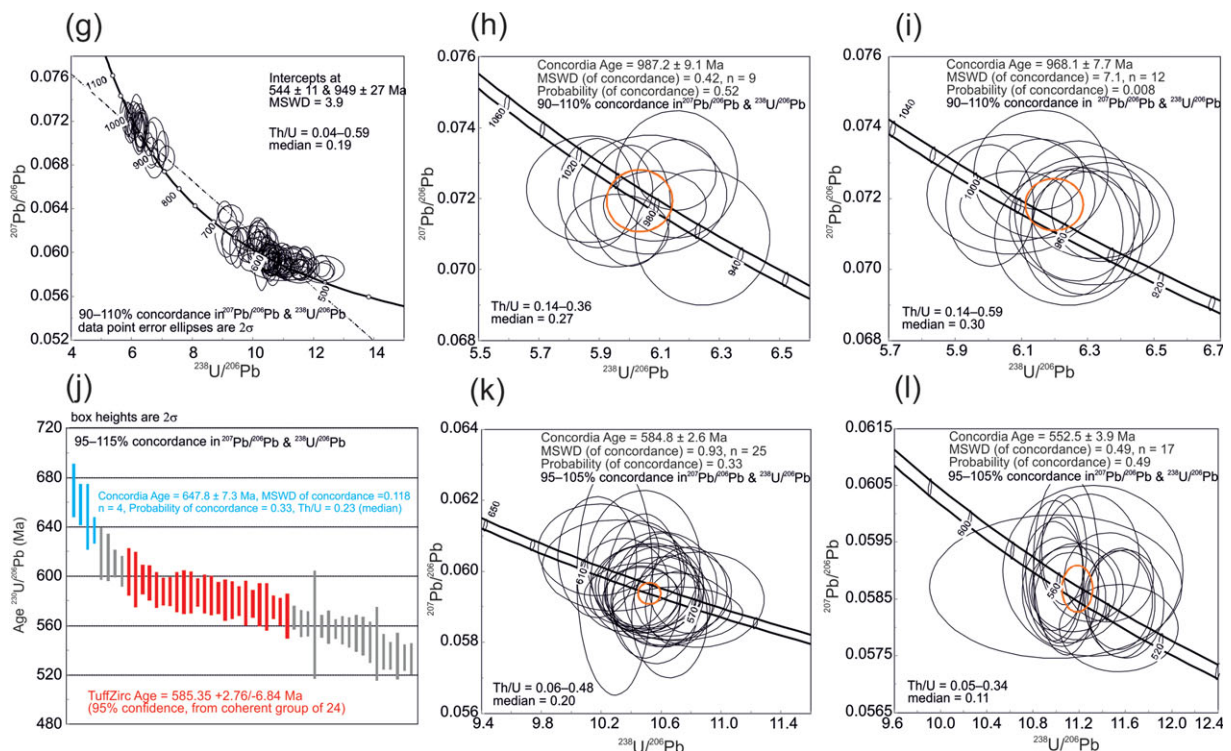
Fig. 6. (Colour online) U–Pb zircon data. Sample 1205A5: (a) Terra-Wasserburg diagram for all data; (b) age distribution of the 95–105% concordant ages with age range defined by the TuffZirc algorithm (in red); and (c) concordia age calculated from the red data in (b). Sample 1217A1: (d) Terra-Wasserburg diagram for all data; (e) age distribution of 95–105% concordant dates and age range defined by the TuffZirc algorithm (in red); the two dates marked in blue may be geologically meaningless or may represent late-stage metamorphic-hydrothermal zircon grains; (f) concordia age calculated from the red data in (e). Sample 1219B1: (g) Terra-Wasserburg diagrams for ages with a level of concordance of 90–110%; upper and lower intercepts through the main age clusters; (h, i) concordia ages for the age groups > 900 Ma; (j) age range defined by the TuffZirc algorithm (in red); the four dates marked in blue may be geologically meaningful, delineating inherited zircons; (k, l) concordia ages for the age groups < 600 Ma.

Table 2. Zircon U–Pb ages

Sample	Lithology	Locality	Latitude (°S)	Longitude (°E)	Age type	Age (Ma)	Uncertainty (Ma ± 2σ or (c. 2%)ᵃ)	MSWD	No. of spots	Th/U median (range)	Age interpretation
1205A5	Monzogranite dyke	Dry Valley N	72.10802	23.18322	Concordia	570.0	1.8 (12)	0.77	38	0.37 (0.19–0.80)	Crystallization
1217A1	Syenite	Lunkeryggen	72.03301	24.59775	Concordia	570.6	3.6 (12)	0.16	11	0.45 (0.21–0.72)	Crystallization
1217A1	Syenite	Lunkeryggen	72.03301	24.59775	Weighted mean	514.0	13.0	0.0048	2	0.06 (0.04–0.08)	Metamorphism
1219B1	Monzogranite dyke	Ridge W of Ellisbreen	72.05848	24.13382	Concordia	987.2	9.1 (20)	0.52	9	0.27 (0.14–0.36)	Inheritance
1219B1	Monzogranite dyke	Ridge W of Ellisbreen	72.05848	24.13382	Concordia	647.8	7.3 13)	0.118	4	0.23 (0.15–0.44)	Inheritance
1219B1	Monzogranite dyke	Ridge W of Ellisbreen	72.05848	24.13382	Concordia	584.8	2.6 (12)	0.93	25	0.20 (0.06–0.48)	Crystallization
1219B1	Monzogranite dyke	Ridge W of Ellisbreen	72.05848	24.13382	Concordia	552.5	3.9 (11)	0.49	17	0.11 (0.05–0.34)	Metamorphism

ᵃTo ensure reproducibility of the reference material, all <2% calculated 2σ crystallization-age uncertainties are reported as 2% in parentheses.
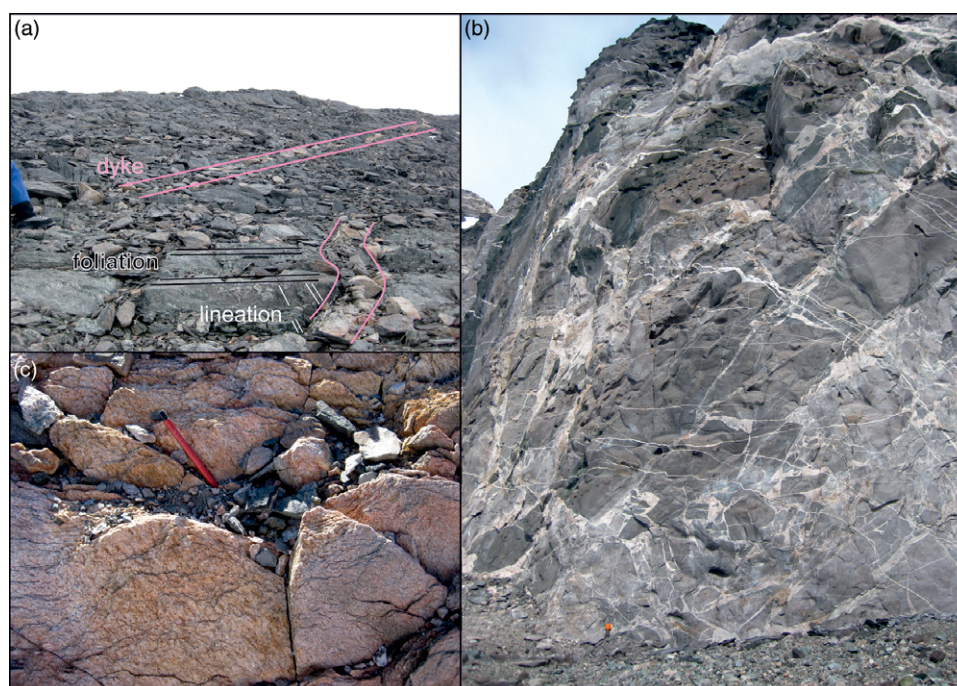

Fig. 7. (Colour online) Field photographs of the dated intrusive rocks. (a) Dry Valley, deformed monzogranitic dyke cuts through mylonitic schist and is offset by a younger oblique reverse fault (1205A5); (b) Lunckeryggen, syenite complex (1217A1) with person for scale; and (c) ridge west of Ellisbreen, monzogranitic dyke with mylonitic texture; pencil indicates stretching lineation (1219B1).

extinction and perthitic exsolution. Quartz, clinopyroxene, titanite, amphibole, biotite and plagioclase occur subordinately. Elburg *et al.* (2016) obtained a weighted mean U–Pb zircon crystallization age of 560 ± 9 Ma (2σ) on a sample from the same area, with inherited age populations at *c.* 617, 715 and 960 Ma.

The zircons dated here are mainly subhedral and round; some are anhedral or occur as fragments. All zircons are < 200 μm in size. Twenty-nine analyses on 25 crystals were performed (Fig. 6d). Analyses younger than *c.* 570 Ma are mostly discordant as a result of Pb loss. The mostly discordant young grains have low Th/U ratios (0.03–0.11) and are dark and featureless

in cathodoluminescence (online Supplementary Fig. S2b). The 95–105% concordant spots yielded a coherent group of 11 dates (out of 16) at $566 + 13/ - 2$ Ma with the TuffZirc algorithm (Fig. 6e). These 11 spots yielded a concordia age of 570.6 ± 3.6 (12) Ma (Fig. 6f). They comprise zircons with partly blured oscillatory and sector zoning. Their Th/U ratios span 0.2–0.7, typical for igneous zircons. Within the 95–105% concordant spots a younger population of ages with two concordant (99 and 100%) outliers yielded a WMA of 514 ± 13 Ma and a Th/U ratio of 0.06. We interpret the concordia age of 571 ± 12 Ma as the syenite crystallization age. The *c.* 514 Ma grains may represent a metamorphic-hydrothermal overprint.

4.b.3. Sample 1219B1, monzogranitic dyke, ridge west of Ellisbreen (72.05848° S; 24.13382° E)

This dyke intruded a grey gneiss and has a mylonitic texture that is parallel to the MSZ (Fig. 7c). The main constituents are quartz, K-feldspar and plagioclase. Quartz occurs in foliation-parallel layers and shows grain-boundary-migration recrystallization. Feldspar forms porphyroclasts with asymmetric pressure shadows of muscovite and minor biotite. Chlorite, illmenite, magnetite and titanite are accessories.

Zircons are subhedral, mainly long prismatic, sometimes round, and reach up to 200 μm in length. Under CL, many zircons show bright and oscillatorily zoned cores surrounded by dark rims, which are either oscillatory zoned or structureless (online Supplementary Fig. S2c). We measured 119 spots that yielded Tonian and Ediacaran age groups (Fig. 6g). The youngest dates generally have higher U contents, probably indicating Pb loss due to metamictization. Two subclusters of the Tonian 90–110% concordant dates yielded concordia ages of 987.2 ± 9.1 (20) and 968.1 ± 7.7 (20) Ma; the respective Th/U ratios are 0.14–0.36 and 0.14–0.59, typical for igneous zircons (Fig. 6h, i).

The Edicarian age population with 95–105% concordance likely contains an older group of four dates from oscillatory-zoned cores at 647.8 ± 7.3 (13) Ma (Th/U ratios = 0.15–0.24). A coherent group of 24 spots yielded a 585.4 + 2.8/ − 6.8 Ma age with the TuffZirc algorithm (Fig. 6j); the concordia age of these mostly oscillatory-zoned cores is 584.8 ± 2.6 (12) Ma and its Th/U ratios span 0.06–0.48 (median = 0.20, Fig. 6k). A younger population of 17 grains yielded a concordia age of 552.5 ± 3.9 (11) Ma; this population comprises mostly rim analyses with weak luminescense and Th/U ratios of 0.05–0.34 (median 0.11, Fig. 6l). All even younger analyses are discordant and have U contents > 2000 ppm.

We interpret the *c.* 585 Ma age as the crystallization age of the dyke; the *c.* 987 and 648 Ma zircon grains as likely inherited, and the *c.* 553 Ma age may represent a metamorphic-hydrothermal overprint. We discard the *c.* 968 Ma age due to the high MSWD of concordance (7.1), which implies that this population also comprises normal discordant grains due to the Ediacaran overprint.

4.c. Cooling rates

Detailed cooling rate determinations are premature as too few thermochronometers have been employed so far. To obtain first-order cooling-rate estimates, we took the following approach. First, the new and published U–Pb zircon ages from our samples are from late-stage, small volume intrusions, that is, pegmatitic granitoids intruding as dykes and sheets. These rocks likely crystallized at relatively low temperatures; we therefore assumed a 650 ± 25 °C crystallization temperature. We then recognized that the Ar/Ar ages are generally much younger than the zircon ages, implying slow cooling. We first assigned classical closure temperatures to the biotite (*c.* 300 °C) and amphibole (*c.* 525 °C) dates and calculated cooling rates from the zircon, amphibole and biotite data for several samples and sample groups. The obtained rates were low, scattering around 10 °C Ma^{-1}. We then recalculated the closure temperatures using the mean of the grain-size range as the effective dimension of the diffusion domain and a range of cooling rates (5–30 °C Ma^{-1}) with the CLOSURE program of Brandon *et al.* (1998). This program applies the parameters given in Grove & Harrison (1996; for biotite) and Harrison (1981; for amphibole). Next, we calculated the final closure temperatures using a cooling rate of 10 °C Ma^{-1} and

assigned uncertainites of ±15 °C, the latter approximating the possible range of values in Sør Rondane (5–30 °C Ma^{-1}). Finally, we calculated error-weighted regressions through dates from single samples and sample groups.

A few first-order features can be derived from these calculations (Fig. 8). The cooling rates through *c.* 700–250 °C are low, around 5–10 °C Ma^{-1} in western Sør Rondane and the northern rim of the SW Terrane S along the MSZ where the database allows calculations; they are probably also low in the NE Terrane. No cooling rate calculations are possible for the CSRC. The biotite ages of the SW Terrane N are distinctly younger than those of the SW Terrane S (with one exception); this may imply an even lower cooling rate for this terrane. The cooling path for the SW Terrane S along the MSZ passes through the *P-T* space of retrograde metamorphic stage M3S (*c.* 400–500 °C at 530–590 Ma; Osanai *et al.* 2013). The cooling path touches the *P-T* space of retrograde metamorphic stage M3N (*c.* 400–550 °C at 530–590 Ma; Osanai *et al.* 2013) in the NE Terrane.

4.d. Summary of new Ar/Ar mineral and U–Pb zircon dating

Twenty-two new Ar/Ar biotite and five new amphibole Ar/Ar ages from five different structural domains span *c.* 570–470 Ma and fall into two main age groups. The older Ar/Ar age group (*c.* 570–525 Ma) is from the MSZ along the northern rim of the SW Terrane S. The younger age group (*c.* 515–470 Ma) is widespread across large parts of the study area but particulary in the SW Terrane N, the NE Terrane and the CSRC. U–Pb zircon data of three granitoids give igneous crystallization ages of *c.* 585, 571 and 570 Ma, with one sample recording inheritance at *c.* 987 and 648 Ma. Two samples record a metamorphic and/or hydrothermal overprint at *c.* 553 and probably 514 Ma. Together with previously published dates for western Sør Rondane (Jacobs *et al.* 2015), our samples span a crystallization age range of 597–528 Ma. Slow cooling rates of 5–10 °C Ma^{-1} characterize Sør Rondane.

5. Discussion

Sør Rondane is mainly underlain by rocks of the TOAST that include GTTG granitoids and their supracrustal cover. There is little evidence for metamorphic overprint before the main granulite-facies metamorphism at *c.* 650–600 Ma. Prior to this high-grade metamorphic overprint, the Tonian oceanic arcs were probably an integral part of the Mozambique Ocean, or had undergone accretion without records of high-grade metamorphism (e.g. Jacobs *et al.* 2015). Granulite-facies metamorphism in the NE Terrane at *c.* 650–600 Ma is thought to relate to overthrusting of the NE Terrane over the SW Terrane along the MTB; this is interpreted from the contrasting *P-T-t* paths on either side of the MTB (Osanai *et al.* 2013), although the MTB itself is largely unexposed. After granulite-facies metamorphism, Sør Rondane underwent amphibolite- to greenschist-facies tectonothermal reworking at *c.* 590–530 Ma (e.g. Shiraishi *et al.* 2008; Osanai *et al.* 2013). With the exception of the MSZ, large parts of the SW Terrane S were only weakly affected by this event (online Supplementary Fig. S3).

Sør Rondane shows pulses of syn- to late-tectonic magmatism at > 600, 580–550, *c.* 530 and 510–500 Ma ('phase one to four'); some of the pulses are unique to one or several of the five distinct tectonic domains (e.g. Shiraishi *et al.* 2008; Elburg *et al.* 2016) (Fig. 9). The interior of the SW Terrane S is only affected by the early, 'phase one' granitoid magmatism, represented by the
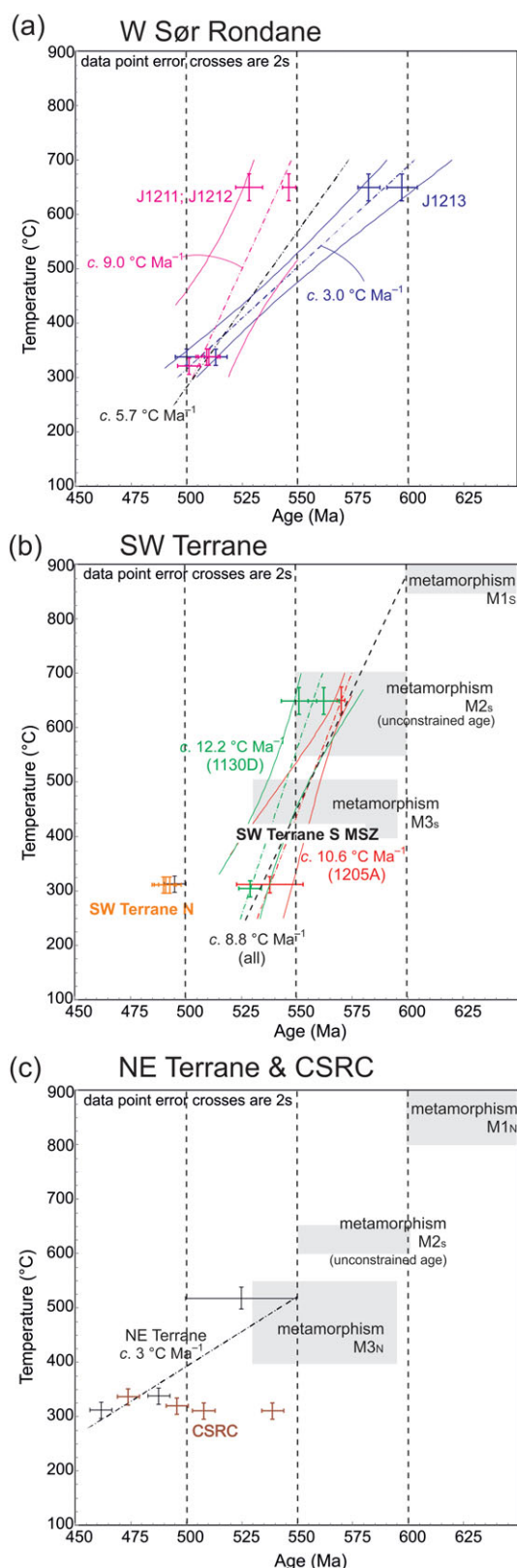
Fig. 8. (Colour online) Cooling-rate estimates. (a) Western Sør Rondane may record slow rates of *c.* 3 °C Ma⁻¹, provided by two pegmatites of 'group 2' magmatism (purple lines); rates of 9 °C Ma⁻¹ are from a migmatite and a gneiss sheet of 'group 3' magmatism (pink lines). The *c.* 5.7 °C Ma⁻¹ rate pools all data. (b) The Main Shear Zone (MSZ) along the northern margin of the SW Terrane S records cooling rates of *c.* 10 °C Ma⁻¹, estimated for two sample groups indicated in red and green (see section 4.a.2 and 4.b). Cooling ages yielded by the samples from the SW Terrane N are indicated; no rate calculations were possible. (c) The cooling rate for the NE Terrane (*c.* 3 °C Ma⁻¹) is only a rough estimate. The wide range of cooling ages provided by the samples from the CSRC is indicated. Grey boxes indicate the *P–T* spaces derived by Osanai *et al.* (2013).

voluminous arc-type Dufek granitoid dated at *c.* 640–620 Ma (Li *et al.* 2006; Elburg *et al.* 2016). The SW Terrane S appears as a rheological stiff tectonic sliver that is surrounded by tectonic domains with significant proportions of rheological weaker metasedimentary rocks; there, 'phase two to four' granitoids occur in significant quantities (Fig. 9). On the one hand, the spatial distribution of our new, as well as the published, Ar/Ar and K–Ar mineral ages appear to reflect the contrasting rheology of the different tectonic domains; on the other hand, they appear to correlate with the spatial distribution of the syn- to late-tectonic granitoid magmatism (Figs 9, S3).

5.a. Cooling history of Sør Rondane

Most Ar/Ar mineral ages of our study post-date both the main granulite-facies metamorphic event at *c.* 650–600 Ma and, to a large extent, also the later amphibolite- to greenschist facies metamorphism at *c.* 590–550 Ma. We interpret the bulk of our Ar/Ar ages to document cooling to below the mineral-specific closure temperatures of *c.* 520–500 °C for amphibole of *c.* 160 µm size and *c.* 340–310 °C for biotite of 250 µm size and a cooling rate of *c.* 10 °C Ma⁻¹, typical for Sør Rondane (see Section 4.c above). Our two main Ar/Ar ages groups of *c.* 570–525 and 515–475 Ma show a clear spatial relation to the five different tectonic domains and the regional distribution of the four phases of granitoids in the region.

The older Ar/Ar age group of *c.* 570–525 Ma is related to the highly sheared northern contact of the SW Terrane S and the MSZ, the tectonic domain where in a previous study a K–Ar mineral age of *c.* 660 Ma was reported (Takigami & Funaki, 1991). The northern margin of the SW Terrane S records significant volumes of 'phase two' granitoid magmatism (*c.* 580–550 Ma), but lacks the two younger granitoid phases. Our new U–Pb zircon crystallization ages from two deformed monzogranitic dykes and one syenite from the MSZ span *c.* 585–570 Ma and correspond to the 'phase two' granitoid magmatism. The late syn- to post-tectonic nature of these intrusions and the metamorphic and/or hydrothermal zircons as young as *c.* 550 Ma imply that the major deformation in the central part of the MSZ was older than *c.* 550 Ma. The rather weak NE-striking foliation of the SW Terrane S that bends into the approximately E-striking MSZ therefore probably pre-dates the 'phase 2' granitoid magmatism (Fig. 9). The new Ar/Ar amphibole (570–550 Ma) and biotite ages (547–524 Ma) of this tectonic domain indicate cooling to below the mineral specific closure temperature after granitoid magmatism, and are therefore interpreted as dating cooling during and after late-stage ductile shearing along the MSZ.

The SW Terrane S is surrounded by four distinct tectonic domains to the north, east and SW, each with contrasting orientations of the main foliation; the orientations differ from those of the SW Terrane S (Fig. 9). All these domains record significantly younger Ar/Ar cooling ages than the SW Terrane S and are dominated by significant volumes of the two later phases of granitoid magmatism at *c.* 530 and 510–500 Ma. 'Phase three' granitoids crop out frequently as small- to moderate-sized bodies throughout these domains; 'phase four' magmatism has so far only been documented in the NE Terrane and west of our study area at Steingarden (Fig. 2; Jacobs *et al.* 2015; Elburg *et al.* 2016). In western Sør Rondane, which is part of the magnetically distinct SE-DML province, the foliation is SE-striking, following the main trend of the dominant magnetic anomalies (Mieth *et al.* 2014). Our five new Ar/Ar biotite ages from this region span 513–500 Ma (Fig. 9), consistent with cooling after the intrusion of 'phase three' granitoids at *c.* 530 Ma. A sixth sample, with an Ar/Ar biotite age of *c.* 503 Ma, was sampled from a moraine (J1221D-1, Jacobs *et al.* 2017), indicating that similar young cooling ages may occur further inland.
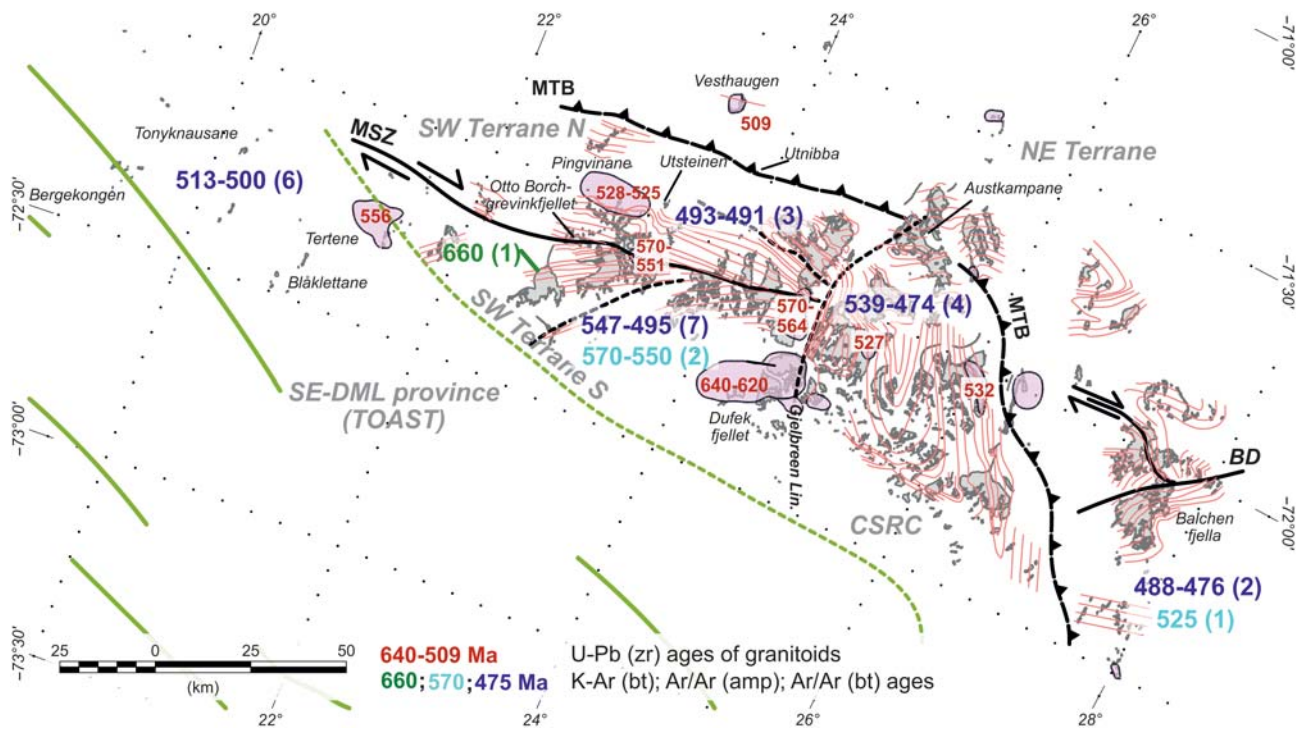
Fig. 9. (Colour online) Summary and overview of the new $^{40}Ar/^{39}Ar$ (this study) and new and published U–Pb zircon crystallization ages of granitoids (pink background) available for Sør Rondane (Elburg *et al.* 2016). Dark green: K–Ar age obtained from Nils Larsenfjellet (Takigami & Funaki, 1991). Black lines: terrane boundaries interpreted based on combined aeromagnetic and geological findings modified after Mieth *et al.* (2014). Green lines: trend of magnetic anomalies within the SE-DML province; dashed line represents assumed southern boundary of the SE Terrane S inferred from aeromagnetic data. Red lines: form line contours based on foliation measurements adapted from Toyoshima *et al.* (2013). Amp – amphibole; bt – biotite; CSCR – central Sør Rondane corridor; MSZ – Main Shear Zone; MTB – Main Tectonic Boundary; zr – zircon.

The SW Terrane N has an overall E-striking foliation, co-linear with the MSZ (Fig. 9). This region records amphibolite- to greenschist-facies metamorphism at 590–530 Ma, which is also documented in the CSRC and in the NE Terrane (Osanai *et al.* 2013). It has a major, 'phase three' granitoid at Utsteinen, dated at *c.* 528 Ma (Elburg *et al.* 2016); Mieth *et al.* 2014). Three of our Ar/Ar biotite cooling ages derive from this domain and span 490–493 Ma, clearly post-dating the 'phase three' granitoid magmatism and possibly indicating post-intrusion cooling in the SW Terrane N.

The NE Terrane is dominated by a mainly E-striking foliation and records large-scale folding, which is related to a compressional phase at *c.* 610 Ma, followed by a transpressional phase and associated dextral shearing (Ishikawa *et al.* 2013). Further, the Balchen extensional detachment (Fig. 9) possibly indicates large-scale extension between 600 and 550 Ma (Ishikawa *et al.* 2013). The NE Terrane exposes only small granitoids that are mostly undated. One granitic dyke at Balchenfjella crystallized at *c.* 549 Ma (Shiraishi *et al.* 2008; online Supplementary Fig. S3d, available at http://journals.cambridge.org/geo); at Vesthaugen, an unde-formed granitoid yielded a crystallization age of *c.* 509 Ma (Elburg *et al.* 2016). Our two new Ar/Ar cooling ages of *c.* 488 and 476 Ma from the eastern part of the NE Terrane are the youngest ages of this study (Fig. 9). These young ages may either account for the thermal effect of the so-far unobserved 'phase four' granitoids in the region or record cooling related to extension after metamorphism in the NE Terrane (Fig. 8c).

The CSRC to the east of both the SW Terrane S and SW Terrane N (east of the Gjelbreen Lineament) has highly variable structural trends and shows large-scale folding (Toyoshima *et al.* 2013).

Magnetic anomaly data indicate that the CSRC may disrupt the MTB into western and eastern parts (Fig. 9; Mieth *et al.* 2014). The CSRS has therefore been interpreted as a domain of major late-tectonic extension (Mieth *et al.* 2014). Two small granitoid bodies within the CSRC crystallized at *c.* 527 and 532 Ma (Elburg *et al.* 2016). Our four Ar/Ar biotite data scatter widely over 474–539 Ma. The oldest Ar/Ar age pre-dates 'phase three' granit-oid magmatism in the CSRC, whereas the remaining ages mainly post-date 'phase four' granitoid magmatism. The widely scattered Ar/Ar ages may be best explained by the complex extensional character of this domain, in which different tectonic levels were juxtaposed.

Each of the five tectonic domains appear to have unique Ar/Ar mineral cooling age signatures that together span *c.* 100 Ma. While the earlier cooling history, as recorded in the SW Terrane S, probably relates to collision of the TOAST with the Kalahari craton and associated magmatic activity and deformation along the MSZ, the later cooling history, as recorded in the NE Terrane and specifically in the CSRC, mostly records extension following orogenic thickening.

In summary, the apparent continuous cooling implied by our data (Fig. 8) for west Sør Rondane and the MSZ along the northern margin of the SW Terrane S supports the suggestion of Adachi *et al.* (2013) that the cooling history is a result of the cooling of the *c.* 570 Ma intrusions and associated regional amphibolite- to greenschist-facies metamorphism. Extrapolation of our cooling rates also yields intersections with the *P-T* space of the granu-lite-facies metamorphism in the NE Terrane; however, this is very speculative (Osanai *et al.* 2013). The most conservative interpreta-tion is that our cooling paths describe a part of the exhumation
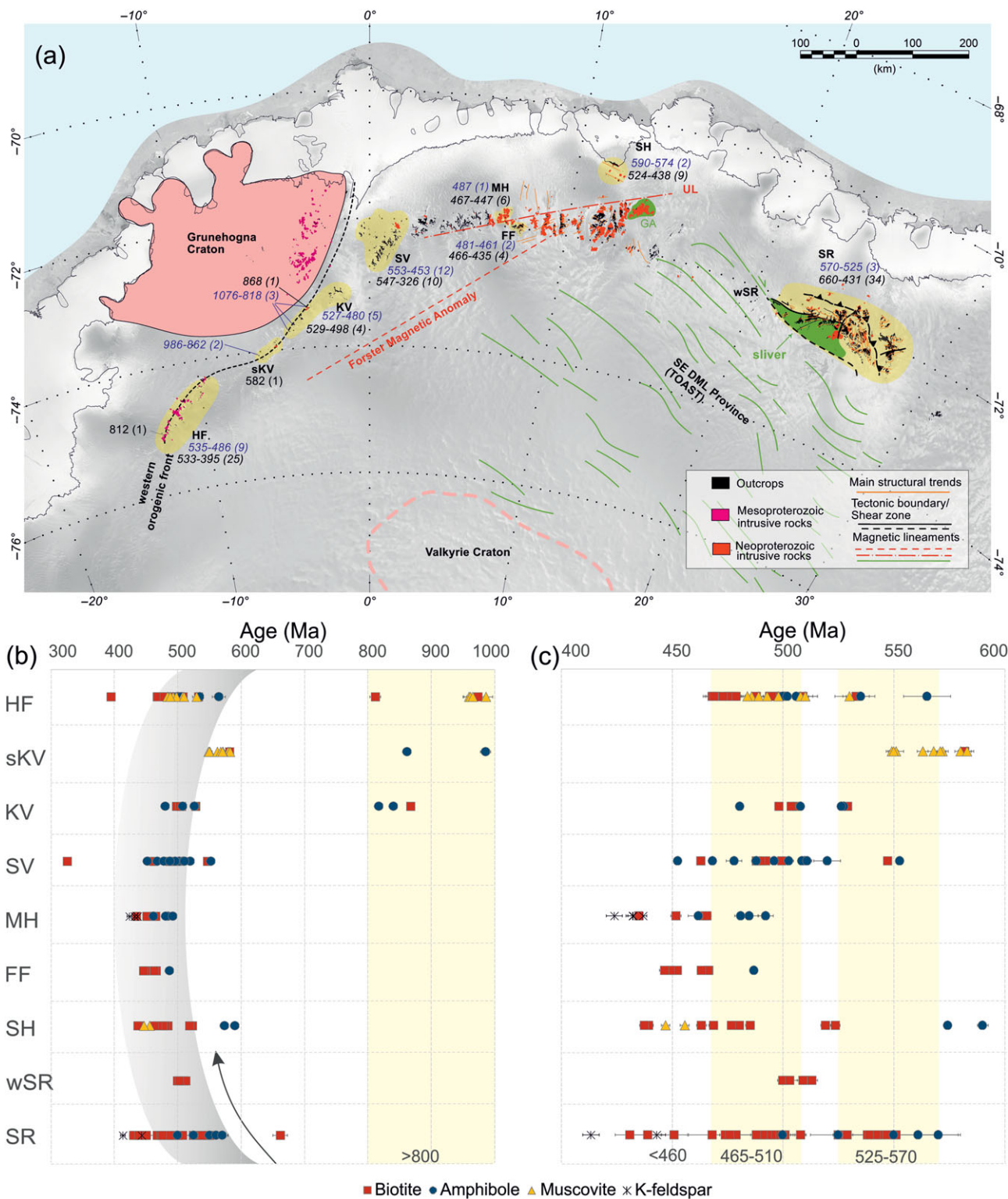
Fig. 10. (Colour online) Overview of cooling ages across Dronning Maud Land. (a) Geographical distribution of the range of amphibole (dark blue numbers) and biotite (black numbers) cooling ages with number of dates in parentheses. (b, c) Summary of cooling ages obtained by K–Ar and ^{40}Ar/^{39}Ar dating for various mineral systems (muscovite, amphibole, biotite and K-feldspar); (c) is a close-up of (b) with a focus on the Ediacarian–Cambrian periods. Data arranged from west to east and uncertainties are quoted at the 2σ confidence level. Age data > 800 Ma only occur to the west of the western orogenic front of the EAAO. Ages < 580 Ma are documented throughout the DML. They reveal a heterogeneous age pattern but outline a general young–old trend from the central DML to the western and eastern DML. FF – Filchnerfjella; GA – Gruber anorthosite; HF – Heimefrontfjella; KV – Kirwanveggen; MH – Mühlig-Hofmann Gebirge; SH – Schirmacher Hills; sKV – southern Kirwanveggen (Urfjell); SR – Sør Rondane; SV – Sverdrupfjella; UL – Ulvetanna Lineament; wSR – western Sør Rondane. Data from Takigami *et al.* (1987), Takigami & Funaki (1991), Jacobs *et al.* (1995, 1999), MRD Croaker, unpubl. MSc thesis, University of Natal (1999), Kleinschmidt *et al.* (2000), WS Board unpub. Ph.D. thesis, University of Capte Town (2001), Helferich *et al.* (2004), Henjes-Kunst (2004), Markl & Henjes-Kunst (2004), Hendriks *et al.* (2013), Grantham *et al.* (2019) and this study.

history of a long-lasting orogeny, including post-contractional erosion and extension. This is supported by the wide age range (597–528 Ma) of the concordant U–Pb zircon dates in our samples that back up the inference that these volumetrically variable and partly regionally confined intrusions appear to have influenced the distinct cooling pattern that we observe in the Sør Rondane region.

5.b. Regional comparison of mineral cooling ages across DML

Comparing our new Ar/Ar mineral cooling ages with published dates across DML, we recognize a number of first-order similarities and differences. As in Sør Rondane, most regions in western and central DML also show Ar/Ar mineral cooling ages of < 530 Ma, specifically in regions characterized by extensive volumes of late-tectonic granitoid magmatism (Fig. 10). The latter has previously been related to delamination tectonics, subsequent to orogenic collapse and an overall associated increased heat flow (e.g. Jacobs *et al.* 2008). Significant older Ar/Ar ages (*c.* 800–1200 Ma) only occur to the west of the western orogenic front of the EAAO, that is, west of the Heimefront Shear Zone (Jacobs *et al.* 1995) and in Kirwanveggen (Kleinschmidt *et al.* 2000; Grantham *et al.* 2019).

As for the SW Terrane S in Sør Rondane, a few other tectonic domains also appear to have escaped the regional collisional tectonometamorphism at *c.* 590–500 Ma in central DML. These domains include the *c.* 600 Ma Gruber anorthosite (Fig. 10), the core of which appears largely undeformed (Jacobs *et al.* 1998) and which has been interpreted as another mega-boudin or tectonic sliver at the boundary between the eastern margin of Kalahari craton and the TOAST (Bauer *et al.* 2004). The Schirmacher tectonic domain also shows little evidence of post-600 Ma tectonothermal overprint, and widely lacks post-600 Ma intrusions (e.g. Henjes-Kunst, 2004; Jacobs *et al.* 2020). It therefore also shows slightly older Ar/Ar cooling ages than the surrounding regions.

In general, Ar/Ar ages of < 580 Ma occur throughout DML and exhibit a heterogeneous age pattern with an overall trend from younger ages in central DML to older ages in its western and eastern parts (Fig. 10). The slightly older Ar/Ar mineral ages along the westernmost EAAO in eastern Heimefrontfjella and in Kirwanveggen coincide with the lack of syn- to post-tectonic granitoid intrusions in the region. In this respect, the western part of the EAAO has similarities with the main part of the SW Terrane S, which similarly lacks syn- to post-tectonic granitoid intrusions and which therefore has comparatively old Ar/Ar ages. As suggested by the data of Adachi *et al.* (2013) and supported by our data (see Section 5.a), the late-tectonic intrusions likely kept the thermal gradient elevated, perhaps supporting ductile extension and keeping the Ar/Ar system open for a prolonged time. This resulted in slow cooling in some parts of central DML (e.g. Markl & Henjes-Kunst, 2004; Hendriks *et al.* 2013). The close relationship of late- to post-tectonic granitoids, comparatively young Ar/Ar ages, high thermal gradients and slow cooling has also been noted in a study from northern Mozambique (Ueda *et al.* 2012), which was positioned adjacent to DML in Gondwana.

The large spread in the Ar/Ar mineral ages and the protracted structural and metamorphic evolution of Sør Rondane and other parts of DML are best explained by a protracted accretionary and collision history that led to the assembly of Gondwana. It is unlikely that a single tectonic mega-event (e.g. Grantham *et al.* 2008, 2013) can explain the age pattern that we record in this study.

The suggested mega-nappe thrust model with top-to-SW thrusting would require a reverse distribution of cooling ages, that is, predominantly older ages in the NE Terrane, representing a nappe/klippe, and younger ages farther to the south or SW in the SW Terrane. This is in contrast to the age zonation in Sør Rondane (Figs 8, S3c).

6. Summary and conclusions

Our new Ar/Ar mineral ages from Sør Rondane span *c.* 570–470 Ma. The data record a protracted cooling history of > 100 Ma that can best be explained by a long-lasting orogeny. The major stages of interlinked tectonic and magmatic processes are as follows.

1. Accretionary tectonics resulted in the formation of the TOAST by the collision of a number of oceanic arc terranes of the Mozambique Ocean, probably outboard the Valkyrie Craton. Two different rheological domains of the TOAST had formed and can now be differentiated: (a) domains predominated by relatively competent igneous rocks (SW Terrane S); and (b) domains dominated by a mixture of rheologically weaker meta-supracrustal cover and arc rocks (remaining areas in the Sør Rondane region). The oldest cooling ages are found in the more competent domains, while the younger age group is found in domains dominated by the meta-supracrustal rocks.

2. Late Neoproterozoic – early Palaeozoic tectonothermal reworking of the TOAST was associated with distinct phases and variable volumes of granitoid intrusions, spanning *c.* 150 Ma. The distribution of our Ar/Ar mineral cooling ages is closely related to these intrusions. The northern margin of the SW Terrane S, the Main Shear Zone, hosts granitoids with three of them newly dated in this study at 584–570 Ma. The new crystallization ages coincide with the second main magmatic period in Sør Rondane that spanned *c.* 580–550 Ma; they provide an age estimate for major deformation along the Main Shear Zone, that is, older than *c.* 550 Ma. Our new Ar/Ar ages (570–524 Ma) record cooling during and after late-stage ductile shearing. This second main magmatic period and deformation along the northern margin of the SW Terrane S may be related to collision of the TOAST with the Kalahari craton. The two younger magmatic events at *c.* 530 Ma and 510–500 Ma are mainly recorded in domains dominated by a mixture of rheologically weaker meta-supracrustal rocks intruded by granitoids; these domains also have the youngest cooling ages. Ages of < 500 Ma predominantly occur in the NE Terrane and in the central Sør Rondane corridor, which are both dominated by late extensional tectonics.

3. The complex, differential and protracted cooling pattern recognized in the five distinct tectonic domains in Sør Rondane are best explained by a protracted collisional history during the final amalgamation of Gondwana. It is unlikely that the structure and cooling pattern seen in the Sør Rondane region and elsewhere in Dronning Maud Land can be resolved by a single large tectonic event such as a mega-nappe thrust model.

References

Adachi T, Osanai Y, Hokada T, Nakano N, Baba S and Toyoshima T (2013) Timing of metamorphism in the central Sør Rondane Mountains, eastern Dronning Maud Land, East Antarctica: constrains from SHRIMP zircon and EPMA monazite dating. *Precambrian Research* **234**, 136–60.

Bauer W, Jacobs J and Paech HJ (2004) Structural evolution of the metamorphic basement of Central Dronning Maud Land, East Antarctica. In *International GeoMaud Expedition of the BGR to Central Dronning Maud Land in 1995/96 - Geological Result* (ed. HJ Paech), pp. 325–63. Hannover: Geologisches Jahrbuch Reihe B.

Boger SD, Hirdes W, Ferreira CAM, Jenett T, Dallwig R and Fanning CM (2015) The 580–520Ma Gondwana suture of Madagascar and its continuation into Antarctica and Africa. *Gondwana Research* **28**, 1048–60.

Brandon MT, Roden-Tice MK and Garver JI (1998) Late Cenozoic exhumation of the Cascadia accretionary wedge in the Olympic Mountains, northwest Washington State. *GSA Bulletin* **110**, 985–1009.

Corfu F, Hanchar JM, Hoskin PWO and Kinny P (2003) Atlas of zircon textures. *Reviews in Mineralogy and Geochemistry* **53**, 469–500.

Deutsch S, Picciotto EE and Reinharz M (1961) Age measurements on Antarctic rocks (Queen Maud Land). *Nature* **191**, 1286–87.

Elburg M, Andersen T, Jacobs J, Läufer A, Ruppel A, Krohne N and Damaske D (2016) One hundred and fifty million years of Pan-African magmatism in the Sør Rondane Mountains (East Antarctica): implications for Gondwana assembly. *The Journal of Geology* **124**, 1–26.

Elburg M, Jacobs J, Andersen T, Clark C, Läufer A, Ruppel A, Krohne N and Damaske D (2015) Early Neoproterozoic metagabbro-tonalite-trondhjemite of Sør Rondane (East Antarctica): implications for supercontinent assembly. *Precambrian Research* **259**, 189–206.

Frei D and Gerdes A (2009) Precise and accurate in situ U–Pb dating of zircon with high sample throughput by automated LA-SF-ICP-MS. *Chemical Geology* **261**, 261–70.

Fretwell P, Pritchard HD, Vaughan DG, Bamber JL, Barrand NE, Bell R, Bianchi C, Bingham RG, Blankenship DD, Casassa G, Catania G, Callens D, Conway H, Cook AJ, Corr HFJ, Damaske D, Damm V, Ferraccioli F, Forsberg R, Fujita S, Gim Y, Gogineni P, Griggs JA, Hindmarsh RCA, Holmlund P, Holt JW, Jacobel RW, Jenkins A, Jokat W, Jordan T, King EC, Kohler J, Krabill W, Riger-Kusk M, Langley KA, Leitchenkov G, Leuschen C, Luyendyk BP, Matsuoka K, Mouginot J, Nitsche FO, Nogi Y, Nost OA, Popov SV, Rignot E, Rippin DM, Rivera A, Roberts J, Ross N, Siegert MJ, Smith AM, Steinhage D, Studinger M, Sun B, Tinto BK, Welch BC, Wilson D, Young DA, Xiangbin C and Zirizzotti A (2013) Bedmap2: improved ice bed, surface and thickness datasets for Antarctica. *The Cryosphere* **7**, 375–93.

Gerdes A and Zeh A (2006) Combined U–Pb and Hf isotope LA-(MC-)ICP-MS analyses of detrital zircons: comparison with SHRIMP and new constraints for the provenance and age of an Armorican metasediment in Central Germany. *Earth and Planetary Science Letters* **249**, 47–61.

Golynsky AV, Ferraccioli F, Hong JK, Golynsky DA, von Frese RRB, Young DA, Blankenship DD, Holt JW, Ivanov SV, Kiselev AV, Masolov VN, Eagles G, Gohl K, Jokat W, Damaske D, Finn C,

Aitken A, Bell RE, Armadillo E, Jordan TA, Greenbaum JS, Bozzo E, Caneva G, Forsberg R, Ghidella M, Galindo-Zaldivar J, Bohoyo F, Martos YM, Nogi Y, Quartini E, Kim HR and Roberts JL (2018) New magnetic anomaly map of the Antarctic. *Geophysical Research Letters* **45**, 6437–49.

Grantham GH, Kramers JD, Eglington B and Burger EP (2019) The Ediacarian-Cambrian uplift history of western Dronning Maud Land: new 40Ar-39Ar and Sr/Nd data from Sverdrupfjella and Kirwanveggen, the source of the Urfjell Group and tectonic evolution of Dronning Maud Land within the Kuunga Orogeny and Gondwana amalgamation. *Precambrian Research* **333**, 105444.

Grantham GH, Macey PH, Horie K, Kawakami T, Ishikawa M, Satish-Kumar M, Tsuchiya N, Graser P and Azevedo S (2013) Comparison of the metamorphic history of the Monapo Complex, northern Mozambique and Balchenfjella and Austhameren areas, Sør Rondane, Antarctica: implications for the Kuunga Orogeny and the amalgamation of N and S Gondwana. *Precambrian Research* **234**, 85–135.

Grantham GH, Macey P, Ingram B, Roberts M, Armstrong R, Hokada T, Shiraishi K, Jackson C, Bisnath A and Manhica V (2008) Terrane correlation between Antarctica, Mozambique and Sri Lanka; comparisons of geochronology, lithology, structure and metamorphism and possible implications for the geology of southern Africa and Antarctica. In *Geodynamic Evolution of East Antarctica: A Key to the East–West Gondwana Connection* (eds M Satish-Kumar, Y Motoyoshi, Y Osani, Y Hiroi and K Shiraishi), pp. 91–119. Geological Society, London, Special Publication no. 308.

Grove M and Harrison TM (1996) 40Ar* diffusion in Fe-rich biotite. *American Mineralogist* **81**, 940–51.

Harrison MT (1981) Diffusion of 40Ar in hornblende. *Contributions to Mineralogy and Petrology* **78**, 324–31.

Helferich S, Läufer AL, Henjes-Kunst F and Kleinschmidt G (2004) Pan-African events in southern Kirwanveggen (western Dronning Maud Land, Antarctica) - evidence from structural geology and geochronology. *Zeitschrift der Deutschen Geologischen Gesellschaft* **154**, 453–68.

Hendriks BWH, Engvik AK and Elvevold S (2013) 40Ar/39Ar record of late Pan–African exhumation of a granulite facies terrain, central Dronning Maud Land, East Antarctica. *Mineralogy and Petrology* **107**, 665–77.

Henjes-Kunst F (2004) Further evidence for Pan-African polyphase magmatism and metamorphism in central Dronning Maud Land, East Antarctica, from rocks at Schirmacheroase: a geochronological study. *Geologisches Jahrbuch Reihe B* **96**, 255.

Higashino F, Kawakami T, Satish-Kumar M, Ishikawa M, Maki K, Tsuchiya N, Grantham GH and Hirata T (2013) Chlorine-rich fluid or melt activity during granulite facies metamorphism in the Late Proterozoic to Cambrian continental collision zone—An example from the Sør Rondane Mountains, East Antarctica. *Precambrian Research* **234**, 229–46.

Hokada T, Horie K, Adachi T, Osanai Y, Nakano N, Baba S and Toyoshima T (2013) Unraveling the metamorphic history at the crossing of Neoproterozoic orogens, Sør Rondane Mountains, East Antarctica: constraints from U–Th–Pb geochronology, petrography, and REE geochemistry. *Precambrian Research* **234**, 183–209.

Ishikawa M, Kawakami T, Satish-Kumar M, Grantham GH, Hokazono Y, Saso M and Tsuchiya N (2013) Late Neoproterozoic extensional detachment in eastern Sør Rondane Mountains, East Antarctica: implications for the collapse of the East African Antarctic Orogen. *Precambrian Research* **234**, 247–56.

Jacobs J, Ahrendt H, Kreutzer H and Weber K (1995) K-Ar, 40Ar-39Ar and apatite fission-track evidence for Neoproterozoic and Mesozoic basement rejuvenation events in the Heimefrontfjella and Mannefallknausane (East Antarctica). *Precambrian Research* **75**, 251–62.

Jacobs J, Bingen B, Thomas RJ, Bauer W, Wingate MTD and Feitio P (2008) Early Palaeozoic orogenic collapse and voluminous late-tectonic magmatism in Dronning Maud Land and Mozambique: insights into the partially delaminated orogenic root of the East African - Antarctic Orogen? In *Geodynamic Evolution of East Antarctica: A Key to the East–West Gondwana Connection* (eds M Satish-Kumar, Y Motoyoshi, Y Osani, Y Hiroi and K Shiraishi), pp. 69–90. Geological Society, London, Special Publication no. 308.

Jacobs J, Elburg M, Läufer A, Kleinhanns IC, Henjes-Kunst F, Estrada S, Ruppel AS, Damaske D, Montero P and Bea F (2015) Two distinct

Late Mesoproterozoic/Early Neoproterozoic basement provinces in central/eastern Dronnning Maud Land, East Antarctica: the missing link, 15-21°E. *Precambrian Research* **265**, 249–72.

Jacobs J, Fanning CM, Henjes-Kunst F, Olesch M and Paech HJ (1998) Continuation of the Mozambique Belt into East Antarctica: Grenville-age metamorphism and polyphase Pan-African high-grade events in central Dronning Maud Land. *The Journal of Geology* **106**, 385–406.

Jacobs J, Hansen B, Henjes-Kunst F, Thomas R, Weber K, Bauer W, Armstrong R and Cornell D (1999) New age constraints on the Proterozoic/Lower Palaeozoic evolution of Heimefrontfjella, East Antarctica, and its bearing on Rodinia/Gondwana correlations. *Terra Antartica* **6**, 377–89.

Jacobs J, Mikhalsky E, Henjes-Kunst F, Läufer A, Thomas RJ, Elburg MA, Wang CC, Estrada S and Skublov S (2020) Neoproterozoic geodynamic evolution of easternmost Kalahari: constraints from U-Pb-Hf-O zircon, Sm-Nd isotope and geochemical data from the Schirmacher Oasis, East Antarctica. *Precambrian Research* **342**, 105553.

Jacobs J, Opås B, Elburg MA, Läufer A, Estrada S, Ksienzyk AK, Damaske D and Hofmann M (2017) Cryptic sub-ice geology revealed by a U-Pb zircon study of glacial till in Dronning Maud Land, East Antarctica. *Precambrian Research* **294**, 1–14.

Jacobs J and Thomas RJ (2004) Himalayan-type indenter-escape tectonics model for the southern part of the late Neoproterozoic-early Paleozoic East African-Antarctic Orogen. *Geology* **32**, 721–24.

Kamei A, Horie K, Owada M, Yuhara M, Nakano N, Osanai Y, Adachi T, Hara Y, Terao M, Teuchi S, Shimura T, Tsukada K, Hokada T, Iwata C, Shiraishi K, Ishizuka H and Takahashi Y (2013) Late Proterozoic juvenile arc metatonalite and adakitic intrusions in the Sør Rondane Mountains, eastern Dronning Maud Land, Antarctica. *Precambrian Research* **234**, 47–62.

Kleinschmidt G, Helferich S, Henjes-Kunst F, Jackson C and Frimmel HE (2000) The pre-Permo-Carboniferous Rocks and Structures from Southern Kirwanveggen, Dronning Maud Land, Antarctica *Polarforschung, Bremerhaven, Alfred Wegener Institute for Polar and Marine Research and German Society of Polar Research* **66**, 7–18.

Krohne N (2017) From Active to Passive Margins: The Basin and Highland Evolution of the Weddell Sea Sector, East Antarctica. Published Ph.D. thesis. University of Bremen.

Lee J-Y, Marti K, Severinghaus JP, Kawamura K, Yoo H-S, Lee JB and Kim JS (2006) A redetermination of the isotopic abundances of atmospheric Ar. *Geochimica et Cosmochimica Acta* **70**, 4507–12.

Li Z, Du Z, Yang S, Chen H, Song B and Liu D (2006) First report of zircon SHRIMP U-Pb dating from the Dufek granite in the Sør Rondane Mountains, East Antarctica. *Journal of Zhejiang University Science A* **7**, 315–19.

Ludwig K (2008) *A User's Manual for Isoplot 3.6. A Geochronological Toolkit for Microsoft Excel.* Berkeley, CA, Berkeley Geochronology Center Special Publication no. 4.

Ludwig K (2012) *User's Manual for Isoplot version 3.75-4.15: A Geochronological Toolkit for Microsoft Excel.* Berkeley, CA, Berkley Geochronological Center, Special Publication no. 5.

Ludwig K and Mundil R (2002) Extracting reliable U-Pb ages and errors from complex populations of zircons from Phanerozoic tuffs. In *Proceedings of 12th Goldschmidt Conference*, Davos, *Geochimica et Cosmochimica Acta* **66**, A463.

Macey PH, Miller JA, Rowe CD, Grantham GH, Siegfried P, Armstrong RA, Kemp J and Bacalau J (2013) Geology of the Monapo Klippe, NE Mozambique and its significance for assembly of central Gondwana. *Precambrian Research* **233**, 259–81.

Mark DF, Stuart FM and de Podesta M (2011) New high-precision measurements of the isotopic composition of atmospheric argon. *Geochimica et Cosmochimica Acta* **75**, 7494–501.

Markl G and Henjes-Kunst F (2004) Magmatic conditions of formation and autometasomatism of post-kinematic charnockites in central Dronning Maud Land, East Antarctica: a model of magmatic evolution. In *International GeoMaud Expedition of the BGR to Central Dronning Maud Land in 1995/96 - Geological Results* (ed. HJ Paech), pp. 139–85. Hannover: Geologisches Jahrbuch Reihe B.

Meert JG (2003) A synopsis of events related to the assembly of eastern Gondwana. *Tectonophysics* **362**, 1–40.

Mieth M, Jacobs J, Ruppel A, Damaske D, Läufer A and Jokat W (2014) New detailed aeromagnetic and geological data of eastern Dronning Maud Land: implications for refining the tectonic and structural framework of Sør Rondane, East Antarctica. *Precambrian Research* **245**, 174–85.

Mieth M and Jokat W (2014) New aeromagnetic view of the geological fabric of southern Dronning Maud Land and Coats Land, East Antarctica. *Gondwana Research* **25**, 358–67.

Osanai Y, Nogi Y, Baba S, Nakano N, Adachi T, Hokada T, Toyoshima T, Owada M, Satish-Kumar M, Kamei A and Kitano I (2013) Geologic evolution of the Sør Rondane Mountains, East Antarctica: collision tectonics proposed based on metamorphic processes and magnetic anomalies. *Precambrian Research* **234**, 8–29.

Otsuji N, Satish-Kumar M, Kamei A, Tsuchiya N, Kawakami T, Ishikawa M and Grantham GH (2013) Late-Tonian to early-Cryogenian apparent depositional ages for metacarbonate rocks from the Sør Rondane Mountains, East Antarctica. *Precambrian Research* **234**, 257–78.

Owada M, Kamei A, Horie K, Shimura T, Yuhara M, Tsukada K, Osanai Y and Baba S (2013) Magmatic history and evolution of continental lithosphere of the Sør Rondane Mountains, eastern Dronning Maud Land, East Antarctica. *Precambrian Research* **234**, 63–84.

Pasteels P and Deutsch S (1963) Age measurements of Antarctic rocks (Queen Maud Land). *Nature* **199**, 996–97.

Pfänder JA, Sperner B, Ratschbacher L, Fischer A, Meyer M, Leistner M and Schaeben H (2014) High-resolution 40Ar/39Ar dating using a mechanical sample transfer system combined with a high-temperature cell for step heating experiments and a multicollector ARGUS noble gas mass spectrometer. *Geochemistry, Geophysics, Geosystems* **15**, 2713–26.

Picciotto E, Deutsch S and Pasteels P (1964) Isotopic ages from the Sør Rondane Mountains, Dronning Maud Land. In *Antarctic Geology: Proceedings of the First International Symposium on Antarctic Geology* (ed. RJ Adie), Cape Town, September 1963, pp. 570–578. North-Holland, Amsterdam: Antarctic Geology.

Renne PR, Mundil R, Balco G, Min K and Ludwig KR (2010) Joint determination of 40K decay constants and 40Ar*/40K for the Fish Canyon sanidine standard, and improved accuracy for 40Ar/39Ar geochronology. *Geochimica et Cosmochimica Acta* **74**, 5349–67.

Riedel S, Jacobs J and Jokat W (2013) Interpretation of new regional aeromagnetic data over Dronning Maud Land (East Antarctica). *Tectonophysics* **585**, 161–71.

Ruppel A, Jacobs J, Eagles G, Läufer A and Jokat W (2018) New geophysical data from a key region in East Antarctica: estimates for the spatial extent of the Tonian Oceanic Arc Super Terrane (TOAST). *Gondwana Research* **59**, 97–107.

Ruppel AS, Läufer A, Jacobs J, Elburg M, Krohne N, Damaske D and Lisker F (2015) The Main Shear Zone in Sør Rondane, East Antarctica: implications for the late-Pan-African tectonic evolution of Dronning Maud Land. *Tectonics* **34**, 1290–305.

Rutte D, Pfänder JA, Koleška M, Jonckheere R and Unterricker S (2015) Radial fast-neutron fluence gradients during rotating 40Ar/39Ar sample irradiation recorded with metallic fluence monitors and geological age standards. *Geochemistry, Geophysics, Geosystems* **16**, 336–45.

Shiraishi K, Dunkley DJ, Hokada T, Fanning CM, Kagami H and Hamamoto T (2008) Geochronological constraints on the Late Proterozoic to Cambrian crustal evolution of eastern Dronning Maud Land, East Antarctica: a synthesis of SHRIMP U-Pb age and Nd model age data. In *Geodynamic Evolution of East Antarctica: A Key to the East–West Gondwana Connection* (eds M Satish-Kumar, Y Motoyoshi, Y Osani, Y Hiroi and K Shiraishi), pp. 21–67. Geological Society, London, Special Publication no. 308.

Sperner B, Jonckheere R and Pfänder JA (2014) Testing the influence of high-voltage mineral liberation on grain size, shape and yield, and on fission track and 40Ar/39Ar dating. *Chemical Geology* **371**, 83–95.

Stacey JS and Kramers JD (1975) Approximation of terrestrial lead isotope evolution by a two-stage model. *Earth and Planetary Science Letters* **26**, 207–21.

Takahashi Y, Arakawa Y, Sakiyama T, Osanai Y and Makimoto H (1990) Rb-Sr and K-Ar whole rock ages of the plutonic bodies from the Sor Rondane Mountains, East Antarctica. *Proceedings of the NIPR Symposium on Antarctic Geosciences* **4**, 1–8.

Takigami Y and Funaki M (1991) $^{40}Ar/^{39}Ar$ and K-Ar ages for igneous and metamorphic rocks from the Sør Rondane Mountains, East Antarctica. *Proceedings of the National Institute of Polar Research Symposium on Antarctic Geosciences* **5**, 122–35.

Takigami Y, Kaneoka I and Funaki M (1987) Age and paleomagnetic studies for intrusive and metamorphic rocks from the Sør Rondane Mountains, Antarctica. *Proceedings of the NIPR Symposium on Antarctic Geosciences* **1**, 169–77.

Toyoshima T, Osanai Y, Baba S, Hokada T, Nakano N, Adachi T, Otsubo M, Ishikawa M and Nogi Y (2013) Sinistral transpressional and extensional tectonics in Dronning Maud Land, East Antarctica, including the Sør Rondane Mountains. *Precambrian Research* **234**, 30–46.

Ueda K, Jacobs J, Thomas RJ, Kosler J, Horstwood MSA, Wartho J-A, Jourdan F, Emmel B and Matola R (2012) Postcollisional high-grade metamorphism, orogenic collapse, and differential cooling of the East African Orogen of Northeast Mozambique. *The Journal of Geology* **120**, 507–30.

Van Autenboer T (1969) Geology of the Sør Rondane Mountains. Geologic Maps of Antarctica (ed. V Buchnell and C Craddock) American Geographical Society (Antarctic Map Folio Series, Folio 12), Sheet 8, Pl. VIII-Sheet 8, Pl. VIII.

Van Autenboer T, Michot J and Picciotto E (1964) Outline of the geology and petrology of the Sør-Rondane Mountains, Dronning Maud Land, in Antarctic Geology. In *Proceedings of the First International Symposium on Antarctic Geology* (ed. RJ Adie), p. 501–14. 16–21 September 1963, Cape Town, North-Holland Publishing Company.